

Response to Anonymous Referee #1

We would like to thank the referee for his/her valuable comments and suggestions which help us improve the quality of the manuscript. All the comments and concerns raised by the referee have been answered carefully point-by point as below and the corresponding parts in the manuscript have been improved.

The original comments are copied here in black color.

Author's responses are in blue color.

All changes to the manuscript have been highlighted with red color in the submitted revised manuscript.

This paper conducted the weather analysis of heavy PM₁₀ pollution events in Chengdu, Deyang, and Mianyang in the northwest Sichuan Basin. Authors extracted major weather patterns, including winds, air temperature, BLH, and pressure system during the occurrence of heavy pollution in this region. The Sichuan Basin is one of several heavily contaminated regions across China and has a typical geographic terrain and persistent weather system. It is necessary to summarize the influences of such the typical terrain and weather system on air pollution prediction in the Basin. To be published in ACP, the paper needs to be improved by addressing following points.

Response: Thank you very much for your positive comments and nice summary.

General comments

1. From my understanding, authors used measured met data in their weather analysis. They highlighted a dry low-pressure system at 700 mb, a warm southerly wind flow, and temperature inversion above the ABL as favorable weather pattern contributing to heavy pollution in their study area. A question might be raised: what is the background weather pattern in Sichuan Basin? Perhaps a better way to present their analysis is to show anomalies of these met variables from their respective long-term means during the deteriorating and improving air quality, instead of real-time measurements, such as figures 2, 4, 5, 8, 9, etc. For example, many readers might not understand what fig.2 is all about because we cannot figure out that wind vectors in this figure are not prevailing winds vectors and if geopotential heights represent the background GH.

Response: Thank you very much for your constructive comments. In order to present our

analysis in a better way, the anomalies of geopotential heights and wind vectors at 700 hPa, the anomalies of west-to-east vertical cross-section of 24-hour temperature change and wind vectors (synthesized by u and w), and the anomalies of temperature vertical profiles were analyzed in the revised manuscript.

To explore the differences between these low-pressure systems and the background of winter atmospheric circulation over there, the anomalies of wind vectors and geopotential heights at 700 hPa were calculated (**Fig. S1**). The calculation method is as follows: the averaged wind vectors and geopotential heights at 700 hPa during periods of deteriorating air quality in the above eight events subtracted from their winter mean values from 1 January 2006 to 31 December 2012 and from 1 January 2014 to 28 February 2017. As illustrated in **Fig. S1**, the anomalies of geopotential heights were negative in the northwest of the urban agglomeration during periods of deteriorating air quality in these heavy air pollution events. As a result, this urban agglomeration was located in front of an anomalous cyclone and was controlled by a strong southerly anomaly wind (**Fig. S1**).

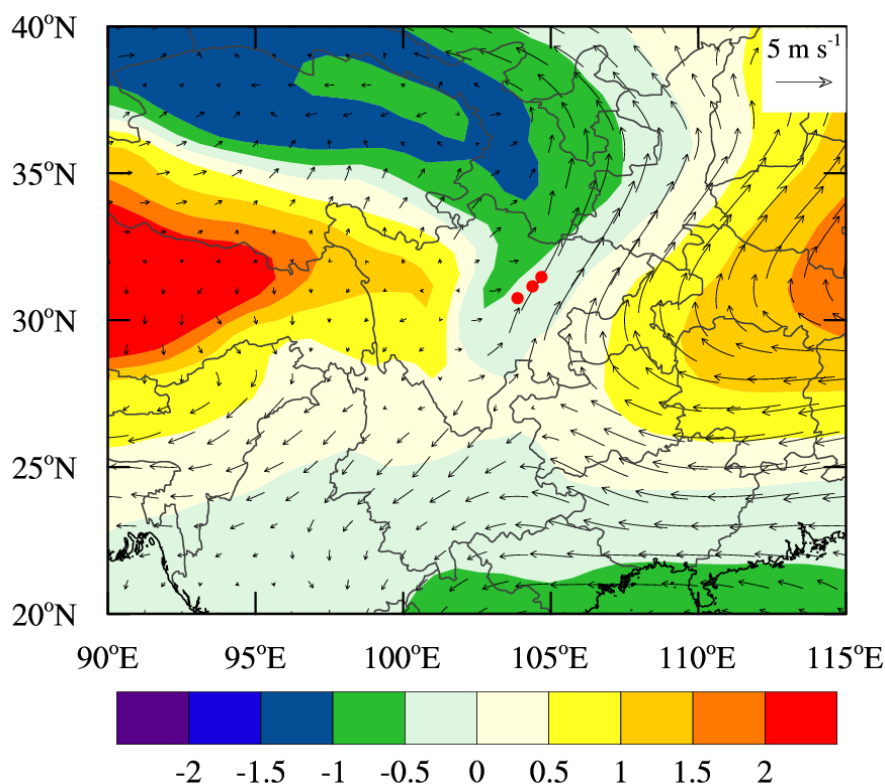


Fig. S1 The anomalies of geopotential heights (shading, units: dagpm) and wind vectors (black arrows) at 700 hPa (the averaged wind vectors and geopotential heights at 700 hPa during periods of deteriorating air quality in the eight heavy air pollution events subtracted from their winter mean values from 1 January 2006 to 31 December 2012 and from 1 January 2014 to 28 February 2017). The red dots show the location of the urban agglomeration.

Additionally, the anomalies of west-to-east vertical cross-section of 24-hour temperature change and wind vectors (synthesized by u and w) (**Fig. S2**), and the anomalies of temperature vertical profiles (**Fig. S3**) were also analyzed to further investigate the influencing mechanism of low-pressure system on heavy air pollution events. **Fig. S2** shows that anomalous warming appeared above the atmospheric boundary layer, while anomalous cooling was observed within the boundary layer when the urban agglomeration was located in front of low-pressure system and was controlled by a southerly warm air flow at 700 hPa. This vertical structure of the anomalies of 24-hour temperature change led to an increase in the stability of the lower troposphere. As illustrated in **Fig. S3**, the positive anomalies of temperature between 1500 m and 3000 m above the ground level increased significantly with height. The maximum value of positive anomalies appeared at about 3000 m and was up to 9 °C. These features revealed that a strong temperature inversion existed above the boundary layer and suppressed the vertical exchange of atmosphere. As a result, the anomalous secondary circulation was also confined in the boundary layer, with its center located at about 925 hPa (**Fig. S2**). These results of anomalies analysis were consistent with the above analysis for real-time data, and further proved that the influencing mechanism of low-pressure system on heavy air pollution events is credible.

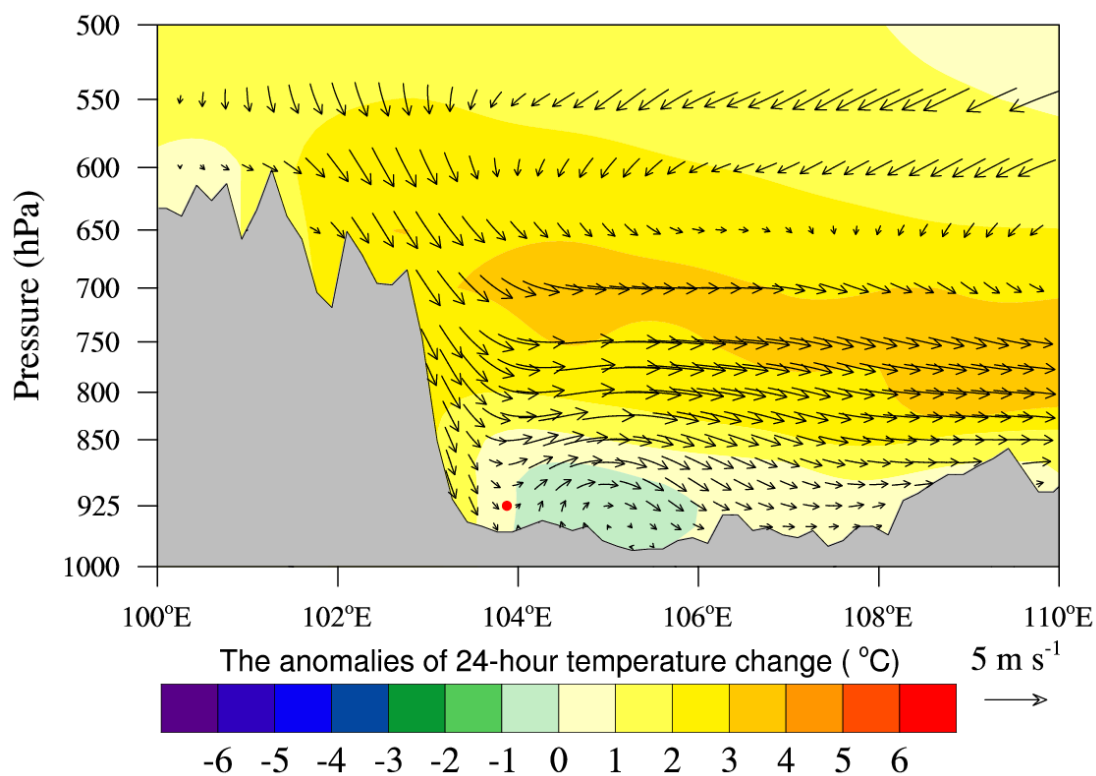


Fig. S2 West-to-east vertical cross-section of the anomalies of 24-hour temperature change and

wind vectors (synthesized by u and w) through the most polluted area (30.75°N) (the averaged 24-hour temperature change and wind vectors during periods of deteriorating air quality in the eight heavy air pollution events subtracted from their winter mean values from 1 January 2006 to 31 December 2012 and from 1 January 2014 to 28 February 2017). Note that the vertical velocity is multiplied by 100 when plotting the wind vectors. The most polluted area is marked by red solid dots. The gray shading represents the terrain.

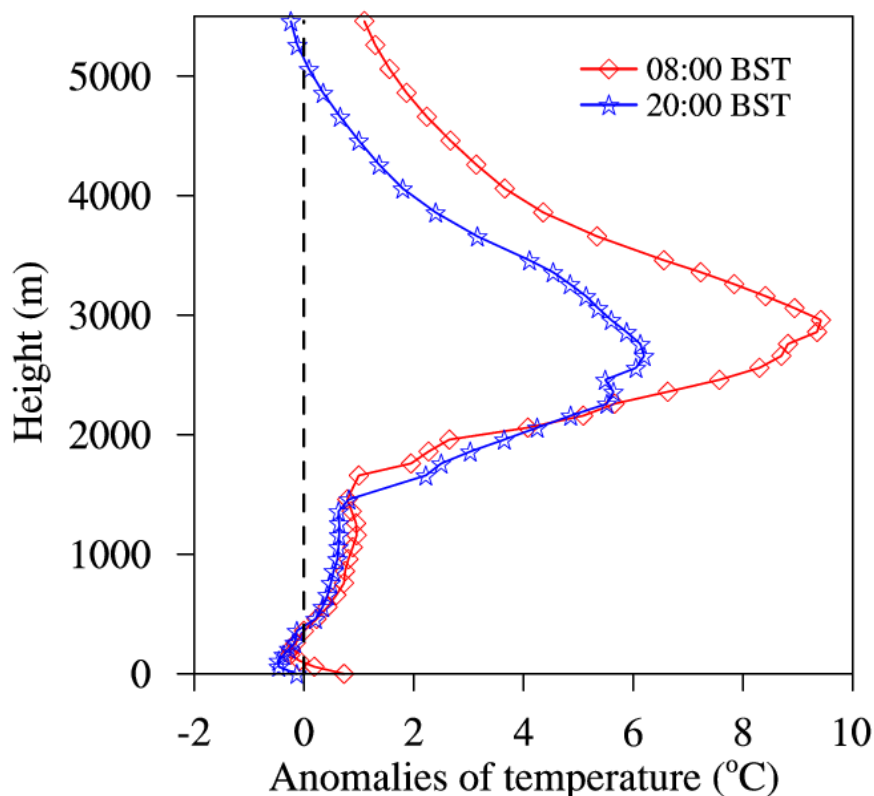


Fig. S3 Vertical profiles of temperature anomalies at Wenjiang station (30.75°N , 103.875°E) measured by radiosonde (the averaged temperature during periods of deteriorating air quality in the eight heavy air pollution events subtracted from their winter mean values from 1 January 2006 to 31 December 2012 and from 1 January 2014 to 28 February 2017).

2. Likewise, Table 2 presents relative vorticity at 700 hPa showing positive in deteriorating air quality but seems not telling readers how these relative vorticities were calculated. Are these departure from the mean averaged over all deteriorating and improving air quality events? Similarly, how were positive and negative BLH, LTS, and MWS in Table 3 estimated?

Response: Thank you very much for your valuable comments. The values of relative vorticity at 700 hPa in **Table 2** and the values of BLH, LTS, and MWS in **Table 3** were not departure from the mean averaged over all deteriorating and improving air quality events. They all were estimated in each of the eight heavy air pollution events. It is considered as a better way to characterize the transits of low-pressure systems for each heavy air pollution event and to estimate the impacts of low-pressure systems on the dispersion capacity of air pollutants in the lower troposphere.

According to your comments, the detailed descriptions of the captions for these met variables in **Table 2** and **Table 3** have been revised as follows:

Table 2. Relative vorticity at 700 hPa during the periods of deteriorating and improving air quality in each of the eight heavy air pollution events.

Table 3. Height of the atmospheric boundary layer (BLH), lower tropospheric stability (LTS), and mean wind speed (MWS) in the lower troposphere during periods of deteriorating air quality in each of the eight heavy air pollution events, and the differences of them between periods of improving and deteriorating air quality in each event.

3. Authors constructed an index based on the results presented in Table 3 to predict the occurrence of heavy air pollution. To demonstrate the usefulness of this index, authors need to apply this index to several independent pollution events and see if the index could successfully forecast heavy pollution in the study area.

Response: Thank you very much for your valuable comments.

First, the index of mean wind speed (MWS) in the lower troposphere was constructed based on the concept of ventilation coefficient, which has been widely used to measure the capability of air pollutants' dispersion in the eastern plains of China (**Deng et al., 2014; Lu et al., 2012; Tang et al., 2015**). Thus, the MWS has a certain physical meaning and rationality. The construction basis and specific method of MWS have been added in the revised manuscript.

Sichuan Basin belongs to a low wind speed zone in China due to its deep mountain-basin topography, and the wind speed in the mixing layer is often low and with small change magnitudes (**Chen and Xie, 2012; Huang et al., 2017; Wang et al., 2018**). For analyzing air quality in Sichuan Basin, the meteorological conditions in the lower troposphere that can reflect ventilation should be considered. To quantitatively evaluate the horizontal dispersion of air pollutants in Sichuan Basin, the mean wind speed (MWS) in the lower troposphere was constructed based on the concept of ventilation coefficient (VC is a product of mixing layer height multiplied by average wind speed through the mixing height). In the eastern plains of China, the ventilation coefficient has been widely used to measure the capability of air pollutants' dispersion (**Deng et al., 2014; Lu et al., 2012; Tang et al., 2015**).

Second, the usefulness of this new index (WMS) have been demonstrated to be good by several independent pollution events. As shown in **Table 3**, the values of this new index (MWS) of

these six events (1–5 and 8) increased significantly after the low-pressure systems had transited the urban agglomeration, and the air quality of these six events improved significantly. For the events 6 and 7 which occurred during the Spring Festival, the improvement of their air quality was mainly attributable to the stop of the letting-off of fireworks. These results revealed that the new index could successfully forecast heavy pollution in the study area.

4. Discussions on Figs. 4 and 8. Discussions and interpretations of these two figures could be improved by clearly describing the lifespan of the low-pressure system and other met conditions during the pollution event. For instance, Fig. 4a shows the beginning of weather pattern causing air pollution and Fig. 4d illustrates the met conditions in the end of pollution event.

Response: Thank you very much for your valuable comments. This manuscript have been revised according your comments.

Other comments

1. Line 123, visibility, how is visibility measured? I don't think visibility helps discussions.

Response: We agree with your comments, and the visibility has been removed in our revised manuscript.

2. Line 143, not clear wind speed on the ground. In terms of no-slip condition, wind speed at the ground surface is zero. Or the wind speed at 10 m height? How many levels from the ground surface to 700 mb? \vec{V} with an upper arrow is wind vector. If Eq 3 denotes wind speed, this upper arrow should be removed.

Response: Thank you very much for your valuable comments. In line 143, the new index (MWS) was calculated based on sounding data which were measured at Wenjiang station (see Fig. 1) in Chengdu. Thus, “Wind speed on the ground” has been revised to “Wind speed at the ground surface”. The vertical levels from the ground surface to 700 mb were not fixed. In general, the number of vertical levels was more than six. The \vec{V} in Eq 3 denotes wind speed, and thus the upper arrow of \vec{V} has been removed in the revised manuscript.

$$MWS = \frac{1}{h} \int_0^h V(z) dz \quad (2)$$

$$\text{MWS} = \frac{1}{h} \sum_{i=1}^n [V_i(z_i) + V_{i-1}(z_{i-1})] \cdot 0.5 \cdot \Delta z_i \quad (3)$$

3. Line 154, any criteria being used to define a “persistent” pollution event?

Response: A “persistent” pollution event was defined by two or more consecutive days with daily PM₁₀ mean concentration $\geq 250 \mu\text{g m}^{-3}$. Moreover, this criteria being used to define a “persistent” pollution event has been added in the revised manuscript.

A “persistent” pollution event was defined by two or more consecutive days with daily PM₁₀ mean concentration $\geq 250 \mu\text{g m}^{-3}$, which is reported to be harmful to the health of local residents (Chow et al., 2006; Guo et al., 2016c; Langrish et al., 2012; Lim et al., 2012).

4. Line 172, in front of low-pressure, better say east or west of the low-pressure system.

Response: Agreed and corrected in the revised manuscript.

5. Line 214, “being” should be “were”

Response: Agreed and corrected in the revised manuscript.

References

- Chen, Y., and Xie, S.: Temporal and spatial visibility trends in the Sichuan Basin, China, 1973 to 2010[J], *Atmos. Res.*, 112, 25-34, <https://doi.org/10.1016/j.atmosres.2012.04.009>, 2012.
- Chow, J. C., Watson, J. G., Mauderly, J. L., Costa, D. L., Wyzga, R. E., Vedal, S., Hidy, G. M., Altshuler, S. L., Marrack, D., Heuss, J. M., Wolff, G. T., Arden Pope Iii, C., and Dockery, D. W.: Health effects of fine particulate air pollution: Lines that connect[J], *J. Air Waste Manage. Assoc.*, 56, 1368-1380, <https://doi.org/10.1080/10473289.2006.10464545>, 2006.
- Deng, T., Wu, D., Deng, X., Tan, H., Li, F., and Liao, B.: A vertical sounding of severe haze process in Guangzhou area[J], *Sci. China Earth Sci.*, 57, 2650-2656, [10.1007/s11430-014-4928-y](https://doi.org/10.1007/s11430-014-4928-y), 2014.
- Guo, Y., Zeng, H., Zheng, R., Li, S., Barnett, A. G., Zhang, S., Zou, X., Huxley, R., Chen, W., and Williams, G.: The association between lung cancer incidence and ambient air pollution in China: A spatiotemporal analysis[J], *Environ. Res.*, 144, 60-65, <https://doi.org/10.1016/j.envres.2015.11.004>, 2016.
- Huang, Q., Cai, X., Song, Y., and Zhu, T.: Air stagnation in China (1985–2014): climatological mean features and trends[J], *Atmos. Chem. Phys.*, 17, 7793-7805, <https://doi.org/10.5194/acp-17-7793-2017>, 2017.
- Langrish, J. P., Li, X., Wang, S., Lee, M. M. Y., Barnes, G. D., Miller, M. R., Cassee, F. R., Boon, N. A., Donaldson, K., Li, J., Li, L., Mills, N. L., Newby, D. E., and Jiang, L.: Reducing personal exposure to particulate air pollution improves cardiovascular health in patients with coronary heart disease[J], *Environ Health Perspect.*, 120, 367-372, <https://doi.org/10.1289/ehp.1103898>, 2012.
- Lim, S. S., Vos, T., Flaxman, A. D., Danaei, G., Shibuya, K., Adair-Rohani, H., AlMazroa, M. A., Amann, M., Anderson, H. R., Andrews, K. G., Aryee, M., Atkinson, C., Bacchus, L. J., Bahalim, A.

N., Balakrishnan, K., Balmes, J., Barker-Collo, S., Baxter, A., Bell, M. L., Blore, J. D., Blyth, F., Bonner, C., Borges, G., Bourne, R., Boussinesq, M., Brauer, M., Brooks, P., Bruce, N. G., Brunekreef, B., Bryan-Hancock, C., Bucello, C., Buchbinder, R., Bull, F., Burnett, R. T., Byers, T. E., Calabria, B., Carapetis, J., Carnahan, E., Chafe, Z., Charlson, F., Chen, H., Chen, J. S., Cheng, A. T.-A., Child, J. C., Cohen, A., Colson, K. E., Cowie, B. C., Darby, S., Darling, S., Davis, A., Degenhardt, L., Dentener, F., Des Jarlais, D. C., Devries, K., Dherani, M., Ding, E. L., Dorsey, E. R., Driscoll, T., Edmond, K., Ali, S. E., Engell, R. E., Erwin, P. J., Fahimi, S., Falder, G., Farzadfar, F., Ferrari, A., Finucane, M. M., Flaxman, S., Fowkes, F. G. R., Freedman, G., Freeman, M. K., Gakidou, E., Ghosh, S., Giovannucci, E., Gmel, G., Graham, K., Grainger, R., Grant, B., Gunnell, D., Gutierrez, H. R., Hall, W., Hoek, H. W., Hogan, A., Hosgood, H. D., Hoy, D., Hu, H., Hubbell, B. J., Hutchings, S. J., Ibeanusi, S. E., Jacklyn, G. L., Jasrasaria, R., Jonas, J. B., Kan, H., Kanis, J. A., Kassebaum, N., Kawakami, N., Khang, Y.-H., Khatibzadeh, S., Khoo, J.-P., Kok, C., Laden, F., Lalloo, R., Lan, Q., Lathlean, T., Leasher, J. L., Leigh, J., Li, Y., Lin, J. K., Lipshultz, S. E., London, S., Lozano, R., Lu, Y., Mak, J., Malekzadeh, R., Mallinger, L., Marcenes, W., March, L., Marks, R., Martin, R., McGale, P., McGrath, J., Mehta, S., Memish, Z. A., Mensah, G. A., Merriman, T. R., Micha, R., Michaud, C., Mishra, V., Hanafiah, K. M., Mokdad, A. A., Morawska, L., Mozaffarian, D., Murphy, T., Naghavi, M., Neal, B., Nelson, P. K., Nolla, J. M., Norman, R., Olives, C., Omer, S. B., Orchard, J., Osborne, R., Ostro, B., Page, A., Pandey, K. D., Parry, C. D. H., Passmore, E., Patra, J., Pearce, N., Pelizzari, P. M., Petzold, M., Phillips, M. R., Pope, D., Pope, C. A., Powles, J., Rao, M., Razavi, H., Rehfuss, E. A., Rehm, J. T., Ritz, B., Rivara, F. P., Roberts, T., Robinson, C., Rodriguez-Portales, J. A., Romieu, I., Room, R., Rosenfeld, L. C., Roy, A., Rushton, L., Salomon, J. A., Sampson, U., Sanchez-Riera, L., Sanman, E., Sapkota, A., Seedat, S., Shi, P., Shield, K., Shivakoti, R., Singh, G. M., Sleet, D. A., Smith, E., Smith, K. R., Stapelberg, N. J. C., Steenland, K., Stöckl, H., Stovner, L. J., Straif, K., Straney, L., Thurston, G. D., Tran, J. H., Van Dingenen, R., van Donkelaar, A., Veerman, J. L., Vijayakumar, L., Weintraub, R., Weissman, M. M., White, R. A., Whiteford, H., Wiersma, S. T., Wilkinson, J. D., Williams, H. C., Williams, W., Wilson, N., Woolf, A. D., Yip, P., Zielinski, J. M., Lopez, A. D., Murray, C. J. L., and Ezzati, M.: A comparative risk assessment of burden of disease and injury attributable to 67 risk factors and risk factor clusters in 21 regions, 1990–2010: a systematic analysis for the Global Burden of Disease Study 2010[J], *Lancet.*, 380, 2224-2260, [https://doi.org/10.1016/S0140-6736\(12\)61766-8](https://doi.org/10.1016/S0140-6736(12)61766-8), 2012.

Lu, C., Deng, Q.-h., Liu, W.-w., Huang, B.-l., and Shi, L.-z.: Characteristics of ventilation coefficient and its impact on urban air pollution[J], *J. Cent. South Univ.*, 19, 615-622, [10.1007/s11771-012-1047-9](https://doi.org/10.1007/s11771-012-1047-9), 2012.

Tang, G., Zhu, X., Hu, B., Xin, J., Wang, L., Münkler, C., Mao, G., and Wang, Y.: Impact of emission controls on air quality in Beijing during APEC 2014: Lidar ceilometer observations[J], *Atmos. Chem. Phys.*, 15, 743-750, <https://doi.org/10.5194/acp-15-12667-2015>, 2015.

Wang, X., Dickinson, R. E., Su, L., Zhou, C., and Wang, K.: PM_{2.5} pollution in China and how it has been exacerbated by terrain and meteorological conditions[J], *Bull. Am. Meteorol. Soc.*, 99, 105-119, [http://dx.doi.org/10.1175/BAMS-D-16-0301.1](https://doi.org/10.1175/BAMS-D-16-0301.1), 2018.

Response to Anonymous Referee #2

Thank you very much for your constructive comments which help us improve the quality of the manuscript. We have carefully modified the manuscript according to your comments. We hope you will be satisfied with our revisions.

The original comments are copied here in black color.

Author's responses are in blue color.

All changes to the manuscript have been highlighted with red color in the submitted revised manuscript.

General comments

Recently, air pollution issues loom large in most parts of China with the development of the economy. Sichuan Basin is one of the seriously polluted areas. This manuscript analyze the relationships between low-pressure systems and heavy air pollution events, and discuss the physical mechanisms of the heavy air pollution in winter in Sichuan basic. The ten heavy air pollution cases were used to analyse over urban agglomeration during 2006-2012 and 2014-2017 in winter, and the eight of those heavy air pollution cases were affected by a dry low-pressure system at 700hPa. When the urban agglomeration is located in front of the low-pressure system, the weather system is controlled by the warm south wind current, and the unstable condition appears at the top of the boundary layer at the same time. The results will be helpful to improve our understanding on environment studies and fall well within the scope of ACP. The minor revisions on the present manuscript are needed before it can be published as followings.

Response: Thank you very much for your positive comments and nice summary.

Minor comments

1. (P.4) Line 120-122: Why the daily average of PM₁₀ is from the last noon to this noon during 2006-2012, but from the last midnight to this midnight during 2014-2017? Please try to describe the purpose.

Response: Thank you very much for your valuable comments.

The third revision of the "Ambient Air Quality Standard" (AAQS) (GB3095-2012) in China was released on February 29th, 2012, replacing the old "Ambient Air Quality Standard" (AAQS) (GB3095-1996). This new standard (GB3095-2012) began to be carried out gradually since 2013.

Thus, the daily average of PM_{10} was from the last noon to this noon during 2006-2012 based on the new “Ambient Air Quality Standard” (AAQS) (GB3095-2012). However, based on the old “Ambient Air Quality Standard” (AAQS) (GB3095-1996), the daily average of PM_{10} was from the last midnight to this midnight during 2014-2017. These detailed descriptions have been added in the revised manuscript.

The third revision of the “Ambient Air Quality Standard” (AAQS) (GB3095-2012) was released on February 29th, 2012, replacing the old “Ambient Air Quality Standard” (AAQS) (GB3095-1996) and $PM_{2.5}$ was adopted into the AAQS in China since 2013. The air quality monitoring stations needed to be updated and the data of air pollutants monitored in the three cities existed missing measurement during 2013. Thus, the winter heavy pollution events during 2013 had not been analyzed in this paper. Moreover, the PM_{10} daily mean concentration from 1 January 2014 to 28 February 2017 refers to the 24-hour average concentration of PM_{10} from 00:00 BST (Beijing Standard Time, i.e., Coordinate Universal Time (UTC) +8 h) to 24:00 BST on the current day based on the new “Ambient Air Quality Standard” (AAQS) (GB3095-2012). However, based on the old “Ambient Air Quality Standard” (AAQS) (GB3095-1996), the PM_{10} daily mean concentration from 1 January 2006 to 31 December 2012 refers to the 24-hour average concentration of PM_{10} from 12:00 BST on the previous day to 12:00 BST on the current day.

2. Fig.2: What time is the result in Fig.2?

Response: Thank you very much for this question. The weather maps at 700 hPa based on ERA-Interim daily data show **Fig. 2(a)** a trough from event 2 at 20:00 BST on 28 January, 2006 and **Fig. 2(b)** a low vortex from event 4 at 14:00 BST on 22 December, 2007. The information is added in the figure caption.

Fig. 2 Weather maps at 700 hPa based on ERA-Interim daily data showing (a) a trough from event 2 at 20:00 BST on 28 January, 2006 and (b) a low vortex from event 4 at 14:00 BST on 22 December, 2007. The blue lines are isopleths of geopotential height, the red lines are isotherms and the black arrows are wind vectors. The green dots show the location of the urban agglomeration.

3. (P8) Line 218: from CASE 3, CASE 4, and CASE 5, the results that is the effect of the low pressure system at 700 hpa causing the value of Boundary Layer height fall. Please describe the reasonableness. We know, the inversion disappears at the higher level, the wind speed increases in

the lower layer, the turbulent motion enhancement, and the boundary layer height increases in the boundary layer when the low-pressure system at 700 hPa passed.

Response: Thank you very much for your valuable comments.

First, Sichuan Basin belongs to a low wind speed zone in China due to its deep mountain-basin topography (**Fig. 1**). The wind speed in the boundary layer is often low and with small change magnitudes (**Chen and Xie, 2012; Huang et al., 2017; Wang et al., 2018**), and the cold air induced by the transit of low-pressure systems usually can't reach in the ground layer (**Fig. 5**). As a result, the increased magnitudes of wind speed (**Fig. 6b, Fig. 7 c and 7d**) and the change magnitudes of temperature (**Fig. 6a, Fig. 7a and 7b**) were very small in the boundary layer after the low-pressure system at 700 hPa passed. Especially for events 3 and 4, the wind speed decreased and a temperature inversion formed in the boundary layer. Thus, the boundary layer heights in air pollution events 3 and 4 decreased after transit of the low-pressure system.

Second, there was a typo in the sentence of “the boundary layer heights in air pollution events 2, 4, and 6 decreased after transit of the low-pressure system”. For event 6 which occurred during the Spring Festival of China, the improvement of its air quality was mainly attributable to the stop of the letting-off of fireworks. As shown in **Table 2** and **Table 3**, the study areas were still located in the front of the low-pressure system and the capacity for dispersion had not yet improved (including the boundary layer height decreased) when the air quality started to improve. Event 6 should be therefore removed in this sentence.

Third, the detailed descriptions about the reasonableness have been added in the revised manuscript according to your comments.

From **Fig.6** and **Fig.7**, we also found some interesting features that the effects of the transit of low-pressure systems at 700 hPa on the meteorological factors within the boundary layer were weak. These features may be related to its deep mountain-basin topography (**Fig. 1**). Under the effects of the deep mountain-basin topography, wind speed in the boundary layer is often low and with small change magnitudes (**Chen and Xie, 2012; Huang et al., 2017; Wang et al., 2018**), and cold air induced by the transit of low-pressure systems usually can't reach to the ground layer (**Fig. 5**). As a result, the increased magnitudes of wind speed (**Fig. 6b, Fig. 7 c and 7d**) and the change magnitudes of temperature (**Fig. 6a, Fig. 7a and 7b**) were very small in the boundary layer after the low-pressure system at 700 hPa passed. Especially for events 3 and 4, the wind speed

decreased and a temperature inversion formed in the boundary layer. These characteristics of the wind and temperature profiles in the boundary layer were the key factors leading to the evolution of boundary layer height as shown in **Table 3**.

4. Table 3, Please add instructions on how to calculate the boundary layer height. The values in the table 3 are average results, right?

Response: Yes, the values in the Table 3 are average results. The height of atmospheric boundary layer was obtained from the ERA-Interim daily dataset at the surface with 3 h temporal resolution (00:00, 03:00, 06:00, 09:00, 12:00, 15:00, 18:00, and 21:00 UTC) (<http://apps.ecmwf.int/datasets/data/interim-full-daily/levtype=sfc/>). This boundary layer height was defined as the level where the bulk Richardson number, based on the difference between quantities at that level and the lowest model level, reaches the critical value $Ri_{cr} = 0.25$ (Beljaars, 2006). The instructions on how to calculate the boundary layer height have been added in the revised manuscript.

5. CASE 6, the whole pollution process lasts a day, but the relative vorticity of air quality is 02:00 on February 3, but the air quality improvement is 14: 00 on February 3 in Table 2. Please confirm the reasonableness of the boundary layer height.

Response: Thank you very much for your valuable comments. The boundary layer height in event 6 has been confirmed to be correct according to your comments. As shown in the response to the third minor comment, in event 6, which occurred during the Spring Festival of China, the improvement of its air quality was mainly attributable to the stop of the letting-off of fireworks. As shown in **Table 2** and **Table 3**, the study areas were still located in the front of the low-pressure system, and the capacity for dispersion has not yet improved (including the decrease in boundary layer height) when the air quality started to improve. The boundary layer height has not increased during the periods of improving air quality in event 6 because the low-pressure system has not yet passed.

6. CASE 6 and 7, the low-pressure system at 700 hPa throughout all the pollution process, the value of pollutant concentration was decreased quickly, why? due to fireworks only? are other processes affecting pollution ?

Response: Thank you very much for this constructive comment.

First, the effects of fireworks on air quality in Chengdu during Chinese New Year (CNY)

from 2013 to 2017 have been investigated. The results showed that time-variations in PM_{10} concentration during CNY were similar in these five years, even though their meteorological conditions were different. As illustrated in **Fig. S4**, PM_{10} concentration increased sharply during the periods of the letting-off of fireworks in CNY, and began to decrease significantly after the letting-off of fireworks stopped. These results were consistent with the changes in particulate pollutant concentrations during CNY in other cities of China (http://www.zhb.gov.cn/gkml/hbb/qt/201702/t20170201_395336.htm). It is a common phenomenon that PM_{10} concentrations decreased sharply after the letting-off of fireworks stopped during CNY. Additionally, to evaluate the effects of excessive emission about fireworks on air quality in a better way, we analyzed the diurnal variations of the differences of averaged PM_{10} concentration in Chengdu between during in the periods of the letting-off of fireworks in CNY (defined as the period from 12:00 BST on the Eve of CNY to 12:00 BST on 1 Lunar January) and 5 days before the letting-off fireworks, and between during 5 days after the letting-off of fireworks in CNY and in the periods of the letting-off of fireworks from 2013 to 2017, see **Fig. S5**. The letting-off of fireworks during CNY was observed to have a significant effect on the air quality in Chengdu. Especially during 5 days after the letting-off of fireworks stopped, production was reduced, factories were shut-down and the numbers of vehicles were lower due to the week-long holiday of CNY (**Liao et al., 2017**). As a result, the maximum decrease in the magnitude of PM_{10} concentration was more than $220 \mu\text{g m}^{-3}$ and occurred at night from 00:00 BST to 06:00 BST (**Fig. S5**) which corresponded to the period of the centralized letting-off of fireworks.

Second, unlike in the normal heavy air pollution events, the concentrations of particulate matter began to decrease sharply in event 6 and 7 before the low-pressure system transited over the urban agglomeration (**Fig. 8**), when the strong temperature inversion still existed above the boundary layer (**Fig. 10**), the local secondary circulation was still confined in the boundary layer (**Fig.9**) and the capacity for dispersion has not yet improved significantly (**Table 3**).

Based on the above analysis results, we conclude that the sharp decreases in PM_{10} concentration for event 6 and 7 were mainly attributable to the significant reduction in emissions induced by the letting-off of fireworks stopped and the week-long holiday of CNY. The detailed discussions had been added in the revised manuscript.

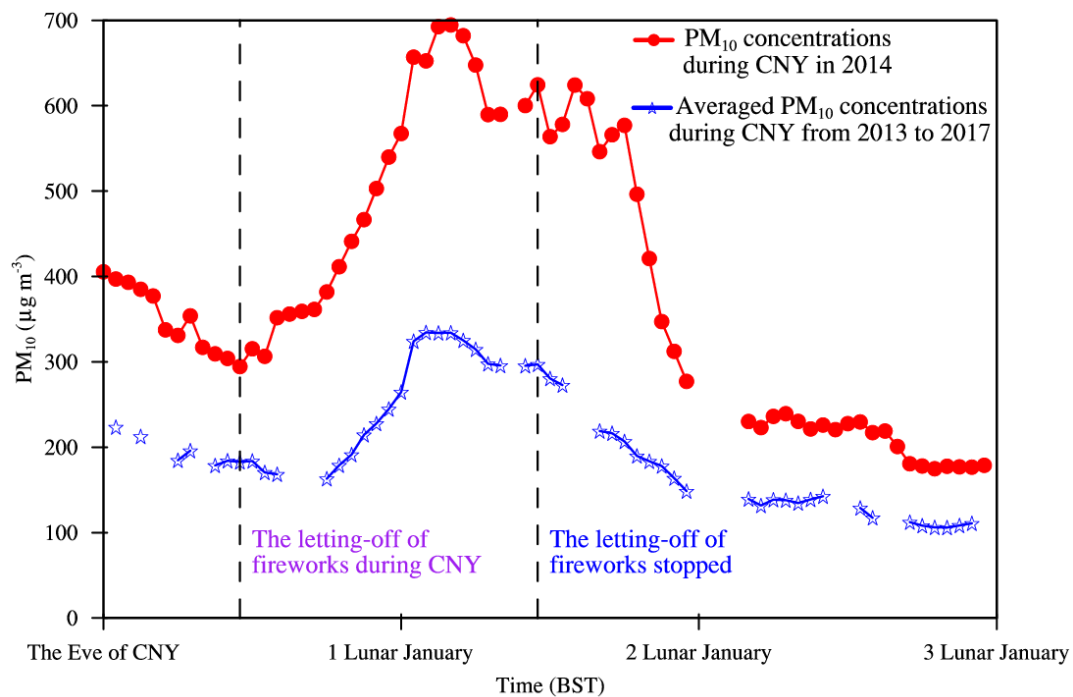


Fig. S4 The hourly concentrations of PM₁₀ during Chinese New Year (CNY) in 2014 for event 7 (red solid line) and the averaged PM₁₀ concentrations during CNY in five years from 2013 to 2017 (blue solid line). Based on Chinese traditional culture, the period from 12:00 BST on the Eve of CNY to 12:00 BST on 1 Lunar January is defined as the letting-off of fireworks during CNY.

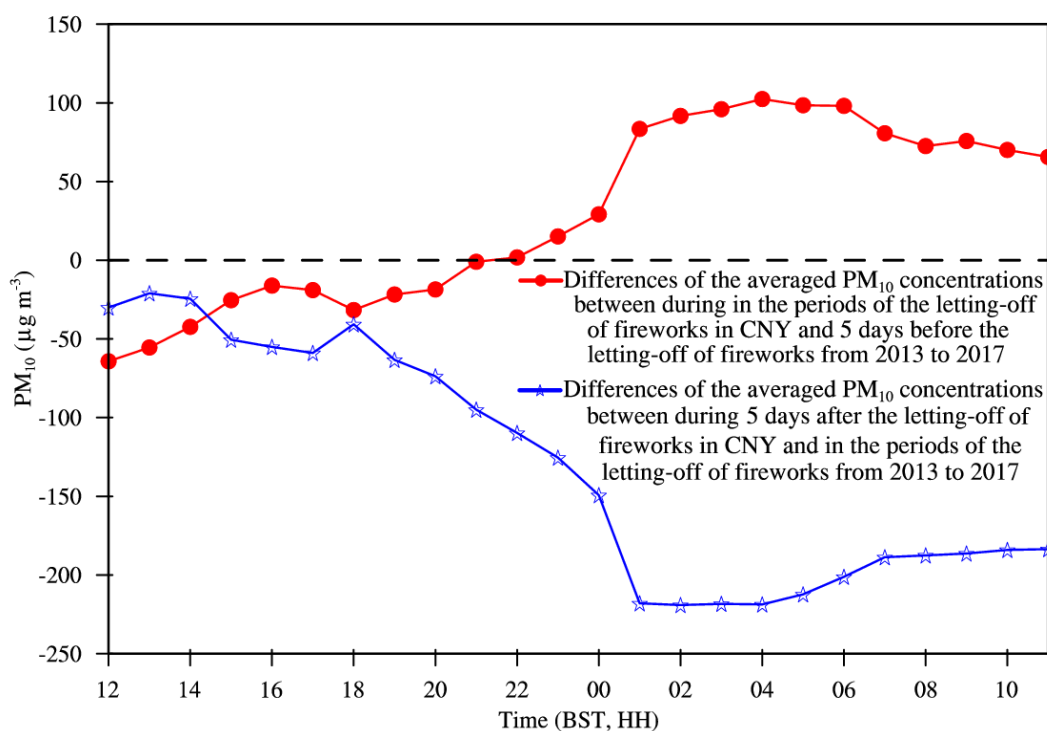


Fig. S5 The diurnal variations of the differences of averaged PM₁₀ concentration in Chengdu between during in the periods of the letting-off of fireworks in CNY and 5 days before the letting-off fireworks (red solid line), and between during 5 days after the letting-off of fireworks in CNY and in the periods of the letting-off of fireworks from 2013 to 2017 (blue solid line). The black dashed line represents zero value.

7. Fig.6, some discussions about the evolution of the PBL height may be also good for a more complete picture.

Response: Thank you very much for this valuable comment. According to your comments, in-depth discussions of **Fig. 6** and **Fig. 7** were added to explain the evolution of PBL height. The detailed discussions had been made in the response to the third minor comment.

8. CASE 6 and CASE 7, the stronger wind shear at 850 hPa means the stronger dynamic turbulence (Fig. 9). How about the characteristics of the wind profile in the boundary layer (refer to Table 3) ?

Response: As shown in the response to the third minor comment, wind speeds in the boundary layer is often low and with small change magnitudes (**Fig. 6b**, **Fig. 7 c** and **7d**). In order to explain the evolution of PBL height in **Table 3**, the characteristics of the wind profile in the boundary layer have been analyzed and added in the revised manuscript.

9. Please unify the format of the references, such as uppercase and lowercase.

Response: the format of the references have been unified according to your comments.

References

- Beljaars, A.: Chapter 3: Turbulent transport and interactions with the surface. Part IV: Physical Processes, IFS Documentation, Operational implementation 12 September 2006 Cy31r1 31, ECMWF, Shinfield Park[J], Reading, RG2 9AX, England, 2006.
- Chen, Y., and Xie, S.: Temporal and spatial visibility trends in the Sichuan Basin, China, 1973 to 2010[J], *Atmos. Res.*, 112, 25-34, <https://doi.org/10.1016/j.atmosres.2012.04.009>, 2012.
- Huang, Q., Cai, X., Song, Y., and Zhu, T.: Air stagnation in China (1985–2014): climatological mean features and trends[J], *Atmos. Chem. Phys.*, 17, 7793-7805, <https://doi.org/10.5194/acp-17-7793-2017>, 2017.
- Liao, T., Wang, S., Ai, J., Gui, K., Duan, B., Zhao, Q., Zhang, X., Jiang, W., and Sun, Y.: Heavy pollution episodes, transport pathways and potential sources of PM_{2.5} during the winter of 2013 in Chengdu (China)[J], *Sci. Total Environ.*, 584-585, 1056-1065, <https://doi.org/10.1016/j.scitotenv.2017.01.160>, 2017.
- Wang, X., Dickinson, R. E., Su, L., Zhou, C., and Wang, K.: PM_{2.5} pollution in China and how it has been exacerbated by terrain and meteorological conditions[J], *Bull. Am. Meteorol. Soc.*, 99, 105-119, <http://dx.doi.org/10.1175/BAMS-D-16-0301.1>, 2018.

1 **Impact of low-pressure systems on winter heavy air pollution in the northwest Sichuan Basin, China**

2 Guicai Ning¹, Shigong Wang^{2,1}, Steve Hung Lam Yim^{3,4,5}, Jixiang Li¹, Yuling Hu¹, Ziwei Shang¹, Jinyan Wang¹, Jiaxin
3 Wang²

4 ¹The Gansu Key Laboratory of Arid Climate Change and Reducing Disaster, College of Atmospheric Sciences,
5 Lanzhou University, Lanzhou 730000, China

6 ²Key Laboratory of Education Bureau of Sichuan Province for Mountain Environmental Meteorology and Public
7 Health, School of Atmospheric Sciences, Chengdu University of Information Technology, Chengdu 610225, China

8 ³Department of Geography and Resource Management, The Chinese University of Hong Kong, Hong Kong, China

9 ⁴The Institute of Environment, Energy and Sustainability, The Chinese University of Hong Kong, Hong Kong, China

10 ⁵[Stanley Ho Big Data Decision Analytics Research Centre, The Chinese University of Hong Kong, Shatin, N.T., Hong
11 Kong, China](#)

12 Correspondence to: Shigong Wang (wangsg@cuit.edu.cn, wangsg@lzu.edu.cn)

13 **Abstract**

14 The cities of Chengdu, Deyang, and Mianyang in the northwest Sichuan Basin are part of a rapidly developing
15 urban agglomeration adjoining the eastern slopes of the Tibetan Plateau. Heavy air pollution events have frequently
16 occurred over the cities in recent decade, but the effects of meteorological conditions on these pollution events are
17 unclear. We explored the effects of weather systems on winter heavy air pollution from 1 January 2006 to 31 December
18 2012 and from 1 January 2014 to 28 February 2017. Ten heavy air pollution events occurred during the research period
19 and eight of these took place while the region was affected by a dry low-pressure system at 700 hPa. When the urban
20 agglomeration was in front of the low-pressure system and the weather conditions were controlled by a warm southerly
21 air flow, and a strong temperature inversion appeared above the atmospheric boundary layer acting as a lid. Forced by
22 this strong inversion layer, the local secondary circulation was confined within the atmospheric boundary layer and the
23 horizontal wind speed in the lower troposphere was low. As a result, vertical mixing and horizontal dispersion in the
24 atmosphere were poor, favoring the formation of heavy air pollution events. After the low-pressure system had
25 transited over the region, the weather conditions in the urban agglomeration were controlled by a dry and cold air flow
26 from the northwest at 700 hPa. The strong inversion layer gradually dissipated, the secondary circulation enhanced and

27 uplifted, and the horizontal wind speed in the lower troposphere also increased, resulting in a sharp decrease in the
28 concentration of air pollutants. The strong inversion layer above the atmospheric boundary layer induced by the
29 low-pressure system at 700 hPa thus played a key role in the formation of heavy air pollution during the winter months
30 in this urban agglomeration. This study provides scientific insights for forecasting heavy air pollution in this region of
31 China.

32 **1 Introduction**

33 Air quality, especially the occurrence of heavy air pollution events, is not only strongly affected by excessive
34 emission of air pollutants, but is also closely associated with meteorological conditions, including atmospheric
35 circulations, weather systems, structures of atmospheric boundary layer, and the corresponding meteorological
36 parameters (Deng et al., 2014;Gu and Yim, 2016;Li et al., 2015;Wei et al., 2011;Ye et al., 2016;Zhang et al.,
37 2012a). The total amount of pollutants emitted in a particular period of time is usually stable in China (Wu et al.,
38 2017), but there are large differences in the concentrations of air pollutants, indicating that the meteorological
39 conditions have an important role in modulating concentrations of ambient air pollutants (Gao et al., 2011;Hu et al.,
40 2014;Ji et al., 2014;Ji et al., 2012;Wang et al., 2010;Wang et al., 2009;Yang et al., 2011).

41 Weather systems control the ability of the atmosphere to disperse pollutants and thus provide the primary driving
42 force for variations in regional air pollution (Chen et al., 2008;Ye et al., 2016). Leśniok et al. (2010) reported that the
43 atmosphere was stagnant and that the concentrations of near-ground air pollutants increased significantly in Upper
44 Silesia, Poland during periods with an anticyclonic circulation. By contrast, when a cyclonic circulation prevailed,
45 causing an inflow of fresh air masses from regions with lower levels of pollution, the concentrations of air pollutants
46 decreased. As synoptic-scale high-pressure ridges at 500 hPa transit across Utah, accompanied by warm advection
47 above valleys, the stability of the atmosphere is increased and favors the formation of persistent pools of cold air,
48 resulting in deterioration in air quality (Whiteman et al., 2014).

49 Many studies have been carried out on the impact of weather systems on air quality in China. Bei et al. (2016)

50 classified typical synoptic situations and evaluated their contributions to air quality in the Guanzhong Basin, China.
51 They found that an inland high-pressure system at 850 hPa resulted in temperature inversion, low horizontal wind
52 speed and a shallow atmospheric boundary layer, which favor the formation of heavy air pollution. Weather systems
53 have significantly impact on the transport of air pollutants. Luo et al. (2018) reported that the trans-boundary air
54 pollution and the pollutant concentration in Hong Kong increased when a tropical cyclones is approaching. During
55 winter, floating dust particles over northwestern China can be carried downstream to northern China by the prevailing
56 northwesterly winds at 700 hPa, where they mix with anthropogenic pollution to form a regional haze (**Tao et al.,**
57 **2012;Tao et al., 2014**). Changes in weather systems also significantly influence air quality. Shallowing of the East
58 Asian trough and weakening of the Siberian high-pressure in winter can induce weak horizontal advection and vertical
59 convection in the lower troposphere, reducing the height of the boundary layer in the Beijing–Tianjin–Hebei region
60 and favoring the formation of haze (**Zhang et al., 2016**).

61 The deep Sichuan Basin to the east of the Tibetan Plateau has a maximum elevation difference >2000 m, and is
62 ranked fourth in China for heavy air pollution after the Beijing–Tianjin–Hebei region, the Yangtze River Delta, and the
63 Pearl River Delta (**Tian et al., 2017;Zhang et al., 2012b**). The complex terrain leads to unique weather systems that
64 affect air quality in this region (**Chen et al., 2014;Huang et al., 2017**). Low-pressure systems, such as a southwest
65 vortex and low trough, are often formed at 700 hPa due to the dynamic and thermodynamic effects of the Tibetan
66 Plateau (**Wang and Tan, 2014;Yu et al., 2016**) and have different characteristics in different seasons. They are warm
67 and moist low-pressure systems in summer and autumn and have crucial effects on local precipitation (**Feng et al.,**
68 **2016;Peng and Cheng, 1992**); much work has been carried out in an attempt to understand the impacts of these
69 low-pressure systems on precipitation (**Chen et al., 2015;Fu et al., 2011;Kuo et al., 1986;Kuo et al., 1988;Ni et al.,**
70 **2017**). In winter and spring, however, these low-pressure systems are both dry and cold (**Feng et al., 2016**). No
71 attempt has previously been made to investigate the association between air quality and these dry and cold
72 low-pressure systems.

73 Chengdu, Deyang, and Mianyang, have undergone rapid development to form an urban agglomeration in the
74 northwest Sichuan Basin. This urban agglomeration lies close to the eastern slopes of Tibetan Plateau, and is affected
75 by low-pressure systems moving east from the plateau (**Feng et al., 2016**). Heavy air pollution events have frequently
76 occurred over there in recent decade. Number of days with exceedance of Grade II standards (**MEP, 2012**) is more
77 than 150 days each year in Chengdu (**Ning et al., 2018**). Most previous studies have investigated the basic
78 characteristics of air pollution (**Chen and Xie, 2012;Chen et al., 2014;Luo et al., 2001;Ning et al., 2018;Tao et al.,**
79 **2013a;Tao et al., 2013b;Zhang et al., 2017**) and the related meteorological parameters (**He et al., 2017;Li et al.,**
80 **2015;Liao et al., 2017;Zeng and Zhang, 2017**). However, the influencing mechanism of dry low-pressure system on
81 heavy air pollution events has yet to be comprehensively explored. The main purpose of this study was to statistically
82 analyze the relationships between low-pressure systems and winter heavy air pollution events in this urban
83 agglomeration, and to explore the physical mechanisms involved in the formation of winter heavy air pollution. This
84 study can deepen our understanding of the meteorological causes of heavy air pollution events in winter, and provide
85 scientific insights that can be used by local governments to take effective measures to mitigate air pollution.

86 This paper is organized as follows. The data and methods are described in Section 2. Section 3 provides a
87 statistical analysis of the relationships between the low-pressure systems and winter heavy air pollution. Section 4
88 illustrates the physical mechanisms of the effect of weather systems on air pollution and our conclusions are
89 summarized in Section 5.

90 **2 Data and methods**

91 **2.1 Air quality data**

92 Air pollution in the Sichuan Basin during the winter months is mainly caused by particulate matter (**Ning et al.,**
93 **2018**). The Chinese Ministry of Environmental Protection (MEP) currently monitors particles with diameters $\leq 2.5 \mu\text{m}$
94 ($\text{PM}_{2.5}$) and particles with diameters $\leq 10 \mu\text{m}$ (PM_{10}). We studied heavy air pollution events occurring during the winter
95 months in Chengdu, Deyang, and Mianyang in the northwest Sichuan Basin (**Fig. 1**). We selected pollution events with

96 a daily PM₁₀ mean concentration $\geq 350 \mu\text{g m}^{-3}$ from 1 January 2006 to 31 December 2012 and from 1 January 2014 to
97 28 February 2017. The third revision of the “Ambient Air Quality Standard” (AAQS) (GB3095-2012) was released on
98 February 29th, 2012, replacing the old “Ambient Air Quality Standard” (AAQS) (GB3095-1996) and PM_{2.5} was
99 adopted into the AAQS in China since 2013. The air quality monitoring stations needed to be updated and the data of
100 air pollutants monitored in the three cities existed missing measurement during 2013. Thus, the winter heavy pollution
101 events during 2013 ~~had~~ have not been analyzed in this paper. Moreover, the PM₁₀ daily mean concentration from 1
102 January 2014 to 28 February 2017 refers to the 24-hour average concentration of PM₁₀ from 00:00 BST (Beijing
103 Standard Time, i.e., Coordinate Universal Time (UTC) +8 h) to 24:00 BST on the current day based on the new
104 “Ambient Air Quality Standard” (AAQS) (GB3095-2012). However, based on the old “Ambient Air Quality Standard”
105 (AAQS) (GB3095-1996), tThe PM₁₀ daily mean concentration from 1 January 2006 to 31 December 2012 refers to the
106 24-hour average concentration of PM₁₀ from 12:00 BST ~~(Beijing Standard Time, i.e., Coordinate Universal Time~~
107 ~~(UTC) +8 h)~~ on the previous day to 12:00 BST on the current day. ~~The PM₁₀ daily mean concentration from 1 January~~
108 ~~2014 to 28 February 2017 refers to the 24-hour average concentration of PM₁₀ from 00:00 BST to 24:00 BST on the~~
109 ~~current day.~~ Hourly concentrations of PM_{2.5}, sulfur dioxide (SO₂), nitrogen dioxide (NO₂), carbon monoxide (CO), and
110 ozone (O₃) were also measured in the three cities from 1 January 2014 to 28 February 2017. These above air quality
111 data were collected from the MEP website (<http://datacenter.mep.gov.cn/index>).

112 **2.2 Meteorological data**

113 **(1) ERA-Interim daily data**

114 To analyze the weather systems at 700 hPa, and the dynamic and thermodynamic conditions in the lower
115 troposphere, the temperature, the geopotential, the vertical velocity, and the u and v components of wind during the
116 study period were obtained from the ERA-Interim daily dataset (0.125° × 0.125° grids) from 950 to 500 hPa for a total
117 of 14 vertical layers (with a vertical separation of 25 hPa from 950 to 775 hPa and a vertical separation of 50 hPa from
118 750 to 500 hPa). These meteorological data are available for 00:00, 06:00, 12:00, and 18:00 UTC and were collected

119 from the website (<http://apps.ecmwf.int/datasets/data/interim-full-daily/levtype=pl/>). The height of the atmospheric
120 boundary layer was obtained from the ERA-Interim daily dataset at the surface with a 3 h temporal resolution (00:00,
121 03:00, 06:00, 09:00, 12:00, 15:00, 18:00, and 21:00 UTC)
122 (<http://apps.ecmwf.int/datasets/data/interim-full-daily/levtype=sfc/>) to explore the structure of the atmospheric
123 boundary layer. This boundary layer height was defined as the level where the bulk Richardson number, based on the
124 difference between quantities at that level and the lowest model level, reaches the critical value $Ri_{cr} = 0.25$ (Beljaars,
125 2006).

126 (2) Sounding data

127 Radiosonde measurements from launches at Wenjiang station (see **Fig. 1**) in Chengdu city (30.70 °N, 103.83 °E,
128 elevation 541.0 m) at 08:00 and 20:00 BST were obtained from the University of Wyoming website
129 (<http://weather.uwyo.edu/upperair/sounding.html>) and included the temperature, potential temperature, and horizontal
130 wind. These data were used to investigate the dynamic and thermodynamic structure of the lower troposphere.

131 ~~(3) Visibility~~

132 ~~Visibility from three observation stations in the three cities was provided by the National Meteorological~~
133 ~~Information Center of the China Meteorological Administration, and was also used in this paper.~~

134 2.3 Quantitative measures of meteorological conditions

135 2.3.1 Lower tropospheric stability

136 The lower tropospheric stability (LTS) is defined as the difference in the potential temperature between 700 hPa
137 and the surface (Slingo, 1987), and can be used to describe the thermodynamic state of the lower troposphere (Guo et
138 al., 2016a; Guo et al., 2016b). The LTS can be used to quantitatively evaluate the vertical mixing of air pollutants in
139 the lower troposphere:

$$140 \text{ LTS} = \theta_{700\text{hPa}} - \theta_{\text{surface}} \quad (1)$$

141 A large LTS represents a high degree of stability in the lower troposphere and indicates the potential for the weak

142 vertical mixing of air pollutants.

143 2.3.2 The mean wind speed in the lower troposphere

144 Sichuan Basin belongs to a low wind speed zone in China due to its deep mountain-basin topography, and the
145 wind speed in the mixing layer is often low and with small change magnitudes (Chen and Xie, 2012;Huang et al.,
146 2017;Wang et al., 2018). For analyzing air quality in Sichuan Basin, the meteorological conditions in the lower
147 troposphere that can reflect ventilation should be considered. To quantitatively evaluate the horizontal dispersion of air
148 pollutants in Sichuan Basin, the mean wind speed (MWS) in the lower troposphere was constructed based on the
149 concept of ventilation coefficient (VC is a product of mixing layer height multiplied by average wind speed through
150 the mixing height). In the eastern plains of China, the ventilation coefficient has been widely used to measure the
151 capability of air pollutants' dispersion (Deng et al., 2014;Lu et al., 2012;Tang et al., 2015). However, Thus, the
152 meteorological conditions above the mixing layer should also be considered in Sichuan Basin. To quantitatively
153 evaluate the horizontal dispersion of air pollutants in Sichuan Basin, the mean wind speed (MWS) in the lower
154 troposphere was constructed based on the concept of ventilation coefficient. The mean wind speed (MWS) in the lower
155 troposphere was defined as:

$$156 \quad \text{MWS} = \frac{1}{h} \int_0^h V(z) dz \quad (2)$$

157 where h is the height above the ground at 700 hPa and $V(z)$ is the wind speed in the lower troposphere. This can be
158 simplified as follows:

$$159 \quad \text{MWS} = \frac{1}{h} \sum_{i=1}^n [V_i(z_i) + V_{i-1}(z_{i-1})] \cdot 0.5 \cdot \Delta z_i \quad (3)$$

160 where n is the number of vertical layers from the ground surface to 700 hPa isobaric layer (including the 700 hPa
161 isobaric layer, and n is greater than 6 in general), $V_i(z_i)$ is the wind speed in a vertical layer (when i=0 represents

162 the wind speed ~~at the ground surface on the ground~~ and v_n represents the wind speed at 700 hPa), and ΔZ_i is the
163 difference in height between the two adjacent vertical layers. A large value of MWS suggests strong horizontal
164 dispersion of air pollutants.

165 3 Heavy air pollution events and weather conditions

166 3.1 Overview of the heavy air pollution events

167 A total of ten heavy winter air pollution events occurred from 1 January 2006 to 31 December 2012 and from 1
168 January 2014 to 28 February 2017 in the urban agglomeration of Chengdu, Deyang, and Mianyang. Nine events were
169 accompanied by a low-pressure system at 700 hPa, and the low-pressure systems in eight events were dry and didn't
170 induce precipitation. This paper explores the impacts of dry low-pressure systems on the eight winter heavy air
171 pollution events (see **Table 1** for a summary of these eight events).

172 **Table 1** shows that there was low visibility during these eight heavy air pollution events in which particulate
173 matter is the primary pollutants. Six of the eight events were classified as persistent air pollution events. A
174 “persistent” pollution event was defined by two or more consecutive days with daily PM_{10} mean concentration ≥ 250
175 $\mu g m^{-3}$, which ~~are~~ is reported to be harmful to the health of local residents (Chow et al., 2006; Guo et al.,
176 2016c; Langrish et al., 2012; Lim et al., 2012), and the longest duration was 10 days. Most of the heavy air pollution
177 events had the characteristics of regional pollution, with five pollution events occurring in multiple cities. Two heavy
178 air pollution events (events 6 and 7) occurred during the Spring Festival, with maximum daily mean PM_{10}
179 concentrations up to 403 and 562 $\mu g m^{-3}$ on the Chinese New Year Day. This suggests that the centralized ~~letting~~
180 ~~letting-off~~ of fireworks during the traditional Chinese Spring Festival, accompanied by poor conditions for the
181 dispersion of air pollution, may lead to a sharp increase in the concentration of particulate pollutants near ground level
182 within a short period of time (Huang et al., 2012; Liao et al., 2017; Shi et al., 2011; Wang et al., 2007).

183 3.2 Weather systems and meteorological conditions during heavy air pollution events

184 An analysis of the synoptic conditions showed that the urban agglomeration was affected by low-pressure systems

185 (low vortex or low trough) at 700 hPa during periods of deteriorating air quality in the eight heavy air pollution events
186 (**Fig. 2**). These studied areas were all located in front of low-pressure systems (east of low-pressure systems) and were
187 controlled by a southerly warm air flow (**Fig. 2**). To explore the differences between these low-pressure systems and
188 the background of winter atmospheric circulation over there, the anomalies of wind vectors and geopotential heights at
189 700 hPa were calculated (Fig. S1). The calculation method is as follows: the averaged wind vectors and geopotential
190 heights at 700 hPa during periods of deteriorating air quality in the above eight events subtracted from their winter
191 mean values from 1 January 2006 to 31 December 2012 and from 1 January 2014 to 28 February 2017. As illustrated
192 in Fig. S1, the anomalies of geopotential heights were negative in the northwest of the urban agglomeration during
193 periods of deteriorating air quality in these heavy air pollution events. As a result, this urban agglomeration was
194 located in front of an anomalous cyclone and was controlled by a strong southerly anomaly wind (Fig. S1).

195 Weather systems can be characterized by their relative vorticity. A positive relative vorticity usually corresponds
196 to a low-pressure system, whereas a negative relative vorticity usually represents a high-pressure system. Thus the
197 relative vorticity at 700 hPa was analyzed during periods of both deteriorating and improving air quality (**Table 2**).
198 ~~Table 2 shows that~~ As shown in Table 2, the relative vorticities at 700 hPa during periods of deteriorating air quality
199 were all positive. This indicated that the study areas were located in front of low-pressure systems at 700 hPa. As a
200 result, a southerly warm air flow dominated at 700 hPa and led to an increase in temperature above the atmospheric
201 boundary layer, which increased atmospheric stability and favored the formation of an air pollution event. During
202 periods of improving air quality, the relative vorticities at 700 hPa of six heavy air pollution events (except for events 6
203 and 7) were negative, showing that the low-pressure systems had transited across the study areas. These areas were
204 thus controlled by a northerly dry, cold air flow at 700 hPa. As a consequence, the temperature above the atmospheric
205 boundary layer decreased and the stability of the atmosphere weakened, which favored the vertical mixing of air
206 pollutants.

207 To explore the impacts of low-pressure systems on the structure of the atmospheric boundary layer, the boundary

208 layer height during periods of deteriorating and improving air quality were analyzed for each heavy air pollution event
209 (**Table 3**). In most of the heavy air pollution events, the height of the boundary layer increased after the low-pressure
210 system had passed across the study area. However, the increase in the height of the boundary layer was not as
211 significant as that seen in Eastern China (**He et al., 2015; Ji et al., 2012; Leng et al., 2016; Qu et al., 2017; Quan et al.,**
212 **2013**) and the boundary layer heights in air pollution events 3, and 4, and 6 decreased after transit of the low-pressure
213 system. These results show that the effects of the transit of low-pressure systems at 700 hPa on the height of the
214 boundary layer were weak, and the causes for the formation of these features will be discussed later. It is therefore
215 difficult to explain the variations in the concentrations of air pollutants in the study areas by considering only the
216 meteorological conditions within the boundary layer.

217 Previous studies have shown that the meteorological conditions above the boundary layer should also be
218 considered (**Guo et al., 2016a; Guo et al., 2016b; Slingo, 1987**). Therefore an index of the MWS in the lower
219 troposphere was proposed and this index, together with the LTS of the eight heavy air pollution events, was further
220 investigated (**Table 3**). The differences in the potential temperature between 700 hPa and the surface during periods of
221 deteriorating air quality in the eight events were all ≥ 18.54 K and the maximum value was 29.45 K, indicating that the
222 lower troposphere was very stable. The MWS was ≤ 4.22 m s⁻¹ for all eight events, with a minimum of 1.91 m s⁻¹.
223 These results show that the low-pressure systems resulted in the stagnation of air in the lower troposphere. After the
224 low-pressure systems had transited the study area, the lower tropospheric stability significantly decreased, with a
225 maximum decrease in the LTS of up to -11.23 K, and the MWS increased. This showed that the arrival of a dry, cold
226 air flow induced by the transit of the low-pressure system significantly weakened the stability of the lower troposphere
227 and increased the wind speed, improving air quality.

228 In events 6 and 7, however, although the study areas were still located in front of the low-pressure system and the
229 capacity for dispersion had not yet improved, the concentrations of particulate matter began to sharply decrease before
230 the transit of the low-pressure system. Both of these events occurred during the Chinese Spring Festival. After the

Chinese New Year Day, the ~~letting-letting~~-off of fireworks stopped and the emission of air pollutants was significantly reduced, resulting in a sharp decrease in the concentration of particulate matter (Liao et al., 2017; Shi et al., 2011; Wang et al., 2007). The decrease in the magnitude of the daily mean concentration of PM₁₀ in event 7 was up to 350 µg m⁻³. These eight heavy air pollution events in the northwest Sichuan Basin can therefore be categorized into two types based on their date of occurrence. The two heavy air pollution events (6 and 7) occurring during the Chinese Spring Festival were categorized as Spring Festival excessive emission heavy air pollution events. The other six events (events 1–5 and 8) were categorized as normal heavy air pollution events.

4 Impacts of low-pressure systems on heavy air pollution events

To further explore the mechanism involved in the formation of heavy air pollution events, with a particular emphasis on the effect of low-pressure systems on air quality, a typical event was selected from the eight events described in the preceding section. The variations in air quality and the dynamic and thermodynamic conditions in the lower troposphere of the selected event were analyzed. Additionally, the impacts of Spring Festival excessive emission on heavy air pollution events were also ~~been~~-investigated.

4.1 The influencing mechanism of low-pressure systems on heavy air pollution events

Heavy air pollution event 8 occurred from 1 January 2017 to 6 January 2017 (Table 3) and the most polluted area was Chengdu. The maximum daily mean concentrations of PM_{2.5} and PM₁₀ occurred on 5 January 2017. The maximum PM₁₀ daily mean concentration in Chengdu was up to 480 µg m⁻³. The concentrations of particulate matter increased sharply (Fig. 3) from 00:00 BST on 3 January 2017 to 00:00 BST on 5 January 2017 and the concentrations of nitrogen dioxide and carbon monoxide also showed an increasing trend. Since 12:00 BST on 5 January 2017, the concentrations of particulate matter decreased significantly (Fig. 3).

Fig. 4 shows the weather maps at 700 hPa during event 8. Fig. 4a shows that there was no low-pressure system at 700 hPa over the urban agglomeration at 02:00 BST on 2 January and there was a dry, cold air flow from the northwest. Soon, as shown in Fig. 4b, A-a low trough was generated at 700 hPa on the west side of the urban agglomeration at

14:00 BST on 2 January 2017, which showed the beginning of low-pressure system causing air pollution. This trough later developed and was enhanced, and the lifespan of this low-pressure system was about 3 days. ~~the~~ The urban agglomeration was still located at the front of the trough and was controlled by a warm, moist air flow from the southwest until 02:00 BST on 5 January 2017 (**Fig. 4b** and **4c**). The concentrations of particulate matter in the urban agglomeration increased sharply and the air quality deteriorated. The trough developed further and a low vortex was formed, which transited across over the study area at 02:00 BST on 5 January 2017 (**Fig. 4d**). The urban agglomeration was then located behind the low vortex and was controlled by a northerly dry, cold air flow (**Fig. 4d**), which illustrated the meteorological conditions in the end of air pollution event. ~~and~~ As a result, the air pollutants were rapidly dispersed.

The west–east vertical cross-sections of the 24-hour change in temperature and wind vectors (u and w) in the most polluted area (30.75 ° N) (**Fig. 5**) and the vertical profiles of temperature and horizontal wind speed (**Fig. 6**) were analyzed to investigate the effects of the low-pressure system on the dynamic and thermodynamic dispersion of air pollutants in the lower troposphere.

Fig.4b and **4c** shows that the urban agglomeration was located in front of the low-pressure system and was controlled by a southerly warm air flow. There was a descending motion between the top of the boundary layer and 500 hPa (**Fig. 5a** and **5b**). Under the effects of warm advection and descending motion, a warming center appeared between 800 and 650 hPa (**Fig. 5a–c**) and the maximum increase in the 24-hour temperature was up to 10 °C (**Fig. 6a**). Weak cooling occurred below 800 hPa, a strong temperature inversion appeared between 775 and 650 hPa (**Fig. 6a**), and the stability of the lower troposphere increased. The urban agglomeration was dominated by the low-pressure system for a long time and a long-lasting strong temperature inversion was therefore induced and maintained above the boundary layer. This was different from the temperature inversion that is often seen within the boundary layer in Eastern China (**Ji et al., 2012;Li and Chan, 2016;Li et al., 2012;Wang et al., 2014;Zhang and Niu, 2016**). The temperature inversion acted as a lid over the boundary layer, suppressing the dispersion of air pollutants. This lid effect

277 restrained vertical mixing in the atmosphere and the local secondary circulation was therefore confined in the boundary
278 layer, with its center located at about 850 hPa (**Fig. 5a–c**). The horizontal wind speed below 800 hPa was $\leq 2 \text{ m s}^{-1}$ (**Fig.**
279 **6b**). These results indicate that vertical mixing and horizontal dispersion were weak, causing accumulation of air
280 pollutants at the ground level. The concentrations of particulate matter then sharply increased to their peak value (**Fig.**
281 **3**), generating a heavy air pollution event.

282 A low vortex and trough at 700 hPa transited across the urban agglomeration and a northwesterly dry, cold air flow
283 prevailed (**Fig. 4d**). Under the influence of the cold air flow, a cooling center appeared between 800 and 650 hPa (**Fig.**
284 **5d**), whereas the air temperature increased below 800 hPa (**Fig. 5d**). As a result, the stability in the lower troposphere
285 was weakened and the strong inversion layer gradually disappeared (**Fig. 6a**). The lid effect above the boundary layer
286 also disappeared, resulting in an increase in the local secondary circulation, the center of which was uplifted to 700
287 hPa (**Fig. 5d**). The horizontal wind speed below 800 hPa also increased (**Fig. 6b**). The air pollutants were able to
288 disperse over a larger space and the vertical mixing and horizontal dispersion were significantly improved. The air
289 quality improved and the heavy air pollution event ended.

290 To verify whether the mechanism involved in the formation of event 8 is used for the others heavy air pollution
291 events, the vertical profiles of temperature and horizontal wind speed in events 1-7 (**Fig. 7**) were explored during the
292 periods of both the low-pressure system controlling and transited over this urban agglomeration. Similar to the event 8,
293 a strong temperature inversion appeared over the study area between 800 and 650 hPa (**Fig. 7a**) when the urban
294 agglomeration was located in the front of low-pressure system and was controlled by a southerly warm air flow at 700
295 hPa. Meanwhile, the horizontal wind speed was low below 800 hPa; the wind speed at all levels below 850 hPa was ≤ 2
296 m s^{-1} (**Fig. 7c**). After the low-pressure system had transited across the urban agglomeration, the strong inversion layer
297 above the boundary layer gradually disappeared (**Fig. 7b**), and the horizontal wind speed in the lower troposphere
298 increased (**Fig. 7d**). Therefore, the influencing mechanism of low-pressure system on heavy air pollution events is
299 common in this urban agglomeration.

300 Additionally, the anomalies of west-to-east vertical cross-section of 24-hour temperature change and wind vectors
301 (synthesized by u and w) (Fig. S2), and the anomalies of temperature vertical profiles (Fig. S3) were also analyzed to
302 further investigate the influencing mechanism of low-pressure system on heavy air pollution events. Fig. S2 shows that
303 anomalous warming appeared above the atmospheric boundary layer, while anomalous cooling was observed within
304 the boundary layer when the urban agglomeration was located in front of low-pressure system and was controlled by a
305 southerly warm air flow at 700 hPa. This vertical structure of the anomalies of 24-hour temperature change led to an
306 increase in the stability of the lower troposphere. As illustrated in Fig. S3, the positive anomalies of temperature
307 between 1500 m and 3000 m above the ground level increased significantly with height. The maximum value of
308 positive anomalies appeared at about 3000 m and was up to 9 °C. These features revealed that a strong temperature
309 inversion existed above the boundary layer and suppressed the vertical exchange of atmosphere. As a result, the
310 anomalous secondary circulation was also confined in the boundary layer, with its center located at about 925 hPa (Fig.
311 S2). These results of anomalies analysis were consistent with the above analysis for real-time data, and further proved
312 that the influencing mechanism of low-pressure system on heavy air pollution events is credible.

313 From Fig.6 and Fig.7, we also found some interesting features that the effects of the transit of low-pressure
314 systems at 700 hPa on the meteorological factors within the boundary layer were weak. These features may be related
315 to its deep mountain-basin topography (Fig. 1). Under the effects of the deep mountain-basin topography, wind speed
316 in the boundary layer is often low and with small change magnitudes (Chen and Xie, 2012;Huang et al., 2017;Wang
317 et al., 2018), and cold air induced by the transit of low-pressure systems usually can't reach in the ground layer (Fig.
318 5). As a result, the increase magnitudes of wind speed (Fig. 6b, Fig. 7 c and 7d) and the change magnitudes of
319 temperature (Fig. 6a, Fig. 7a and 7b) were very small in the boundary layer after the low-pressure system at 700 hPa
320 passed. Especially for events 3 and 4, the wind speed decreased and a temperature inversion formed in the boundary
321 layer. These characteristics of the wind and temperature profiles in the boundary layer were the key factors leading to
322 the evolution of boundary layer height in Table 3.

4.2 Impacts of Spring Festival excessive emission on heavy air pollution events

Table 1 shows that events 6 and 7 occurred during the Chinese Spring Festival when the concentration of particulate matter increased sharply. Low concentrations of gaseous pollutants were found throughout these two events, however, which may be related to a reduction in production or the shut-down of factories, as well as lower numbers of vehicles during the week-long Spring Festival (Liao et al., 2017). The centralized ~~letting~~-letting-off of fireworks during the Chinese Spring Festival played an important part in the sharp increase in the concentrations of particulate matter (Huang et al., 2012;Liao et al., 2017;Shi et al., 2011;Wang et al., 2007). We investigated the impacts of Spring Festival excessive emission on event 6 and 7.

It's noteworthy that the emission of air pollutants increased sharply during this period of deteriorating air quality for event 6 and 7 due to the centralized ~~letting~~-letting-off of fireworks during the Chinese Spring Festival. What's more, under the effects of low-pressure system, the strong temperature inversion appeared above the atmospheric boundary layer (Fig. 7a) and the horizontal wind speed was low below 800 hPa (Fig. 7c). The combination of excessive emissions with poor dispersion conditions resulted in the maximum daily concentrations of PM₁₀ occurring on the Chinese New Year Day (Table 1). The maximum daily mean PM₁₀ concentration of eight heavy air pollution events occurred in event 7 and was up to 562 $\mu\text{g m}^{-3}$ (Table 1). This shows that the excessive emissions during the short Chinese Spring Festival were able to increase the peak concentrations of particulate matter. Thus, the centralized letting-off of fireworks in the Chinese Spring Festival combined with the impacts of low-pressure system were the main causes of these two events in this region of China.

Unlike in the normal heavy air pollution events, the concentrations of particulate matter began to decrease sharply in event 6 and 7 before the low-pressure system transited over the urban agglomeration (Fig. 8a and 8b), when the strong temperature inversion was still present above the atmospheric boundary layer (Fig. 10) ~~and~~, the local secondary circulation was still confined in the atmospheric boundary layer (Fig. 9a and 9b) and the capacity for dispersion has not yet improved significantly (Table 3). To explore the causes of the sharp decrease in PM₁₀ concentration for these

346 two events, the effects of fireworks on air quality in Chengdu during Chinese New Year (CNY) from 2013 to 2017
347 have been investigated. The results showed that time-variations of PM₁₀ concentration during CNY were similar in
348 these five years, even though their meteorological conditions were different. As illustrated in Fig. S4, PM₁₀
349 concentration increased sharply during the periods of the letting-off of fireworks in CNY, and began to decrease
350 significantly after the letting-off of fireworks stopped. These results were consistent with the changes of particulate
351 pollutant concentrations during CNY in other cities of China
352 (http://www.zhb.gov.cn/gkml/hbb/qt/201702/t20170201_395336.htm). It is a common phenomenon that PM₁₀
353 concentrations decreased sharply after the letting-off of fireworks stopped during CNY. Additionally, the diurnal
354 variations of the differences of averaged PM₁₀ concentration in Chengdu between during in the periods of the
355 letting-off of fireworks in CNY (defined as the period from 12:00 BST on the Eve of CNY to 12:00 BST on 1 Lunar
356 January) and 5 days before the letting-off fireworks, and between during 5 days after the letting-off of fireworks in
357 CNY and in the periods of the letting-off of fireworks from 2013 to 2017 have been also analyzed (Fig. S5) to evaluate
358 the effects of excessive emission about fireworks on air quality in a better way. As shown in Fig. S5, the letting-off of
359 fireworks during CNY had a significant effect on the air quality in Chengdu. Especially during 5 days after the
360 letting-off of fireworks stopped, production was reduced, factories were shut-down and the numbers of vehicles were
361 lower due to the week-long holiday of CNY (Liao et al., 2017). As a result, the maximum decrease in the magnitude of
362 PM₁₀ concentration was more than 220 μg m⁻³ and occurred at night from 00:00 BST to 06:00 BST (Fig. S5) which
363 corresponded to the period of the centralized letting-off of fireworks. Based on the above analysis results, we found
364 that the sharp decreases in PM₁₀ concentration for event 6 and 7 were mainly attributable to the significant reduction in
365 emissions induced by the letting-off of fireworks stopped and the week-long holiday of CNY. This indicated that these
366 two events were strongly dependent on emissions. Thus, the centralized letting-off of fireworks in the Chinese Spring
367 Festival combined with the impacts of low-pressure system were the main causes of these two events in this region of
368 China.

369 **5 Conclusions and discussions**

370 We investigated the relationships between low-pressure systems and winter heavy air pollution events in the
371 urban agglomeration of Chengdu, Deyang, and Mianyang in the northwest Sichuan Basin and explored the influence of
372 dry and cold low-pressure systems on winter air quality.

373 A total of ten heavy winter air pollution events occurred in the urban agglomeration from 1 January 2006 to 31
374 December 2012 and from 1 January 2014 to 28 February 2017. The meteorological causes of eight of these air
375 pollution events were attributed to dry low-pressure systems (trough and low vortex) at 700 hPa. The schematic
376 diagram in **Fig. 11** shows that a strong temperature inversion appeared above the atmospheric boundary layer because
377 the urban agglomeration was located in front of low-pressure system at 700 hPa and was controlled by a warm
378 southerly air flow. This strong inversion layer acted as a lid over the boundary layer and suppressed the dispersion of
379 air pollutants, confining the local secondary circulation within the atmospheric boundary layer. The horizontal wind
380 speed in the lower troposphere was low. As a result, the space available for the vertical and horizontal dispersion of air
381 pollutants was small. The concentrations of air pollutants increased to their peak values, resulting in heavy air
382 pollution events.

383 After the low-pressure system had transited across the urban agglomeration, the strong inversion layer above the
384 boundary layer gradually disappeared, resulting in an increase and uplift of the secondary circulation and an increase in
385 the horizontal wind speed in the lower troposphere. The space available for the vertical and horizontal dispersion of air
386 pollutants increased and the concentrations of air pollutants decreased sharply, ending the heavy air pollution event.
387 The centralized ~~letting-letting~~-off of fireworks during the Chinese Spring Festival was one of the main causes of the
388 heavy air pollution events in this region of China.

389 The urban agglomeration studied here, which is flanked by the eastern slopes of the Tibetan Plateau, is sensitive
390 to low-pressure systems moving east from the plateau (**Feng et al., 2016**). The complex terrain forms local secondary
391 circulations, which have a significant impact on air quality (**Chen et al., 2009; Liu et al., 2009; Miao et al., 2015**). We

392 found that the intensity and altitude of the local secondary circulations were markedly affected by the low-pressure
393 system and changes in circulation affected the local air quality. The mechanism of influence of the low-pressure
394 system on the local secondary circulation requires further elaboration using numerical simulation. The centralized
395 ~~letting-letting~~-off of fireworks during the Chinese Spring Festival significantly affected the air quality (**Huang et al.,**
396 **2012;Liao et al., 2017;Shi et al., 2011;Wang et al., 2007**), especially during some of the heavy air pollution events in
397 the urban agglomeration, although the impact of fireworks on air quality was remarkably different depending on the
398 dispersion conditions (**Li et al., 2006**). Sensitivity research should therefore be carried out using models coupled with
399 detailed meteorological and chemical processes to quantitatively examine the impacts of the centralized emission of air
400 pollutants from the Chinese Spring Festival on local air quality.

401 **Competing interests**

402 The authors declare that they have no conflict of interest.

403 **Acknowledgements**

404 This work was supported by the National Natural Science Foundation of China (91644226, 41575138), the National
405 Key Research Project of China-Strategy on Black Carbon Reduction and Evaluation of the Health Effects of Climate
406 Change (2016YFA0602004), the Improvement on Competitiveness in Hiring New Faculties Fund (2013/14) of The
407 Chinese University of Hong Kong and the Vice-Chancellor's Discretionary Fund of The Chinese University of Hong
408 Kong (4930744). We would like to thank the following departments for the provided data, the Ministry of
409 Environmental Protection of the People's Republic of China, the European Centre for Medium-Range Weather
410 Forecasts, the University of Wyoming and the China Meteorological Administration. [Anonymous reviewers who](#)
411 [provided comments and suggestions are gratefully acknowledged.](#)

412 **References**

- 413 Bei, N., Li, G., Huang, R. J., Cao, J., Meng, N., Feng, T., Liu, S., Zhang, T., Zhang, Q., and Molina, L. T.: Typical synoptic
414 situations and their impacts on the wintertime air pollution in the Guanzhong basin, China[J], Atmos. Chem. Phys., 16,
415 7373-7387, <https://doi.org/10.5194/acp-16-7373-2016>, 2016.
- 416 Beljaars, A.: Chapter 3: Turbulent transport and interactions with the surface. Part IV: Physical Processes, IFS
417 Documentation, Operational implementation 12 September 2006 Cy31r1 31, ECMWF, Shinfield Park[J], Reading, RG2
418 9AX, England, 2006.
- 419 Chen, Y., Li, Y., and Zhao, T.: Cause ~~Analysis-analysis~~ on ~~Eastward-eastward Movement-movement~~ of Southwest China
420 ~~Vortex-vortex~~ and ~~Its-its Induced-induced Heavy-heavy Rainfall-rainfall~~ in South China[J], Adv Meteorol., 2015, 22,
421 <https://doi.org/10.1155/2015/481735>, 2015.
- 422 Chen, Y., and Xie, S.: Temporal and spatial visibility trends in the Sichuan Basin, China, 1973 to 2010[J], Atmos. Res., 112,
423 25-34, <https://doi.org/10.1016/j.atmosres.2012.04.009>, 2012.
- 424 Chen, Y., Xie, S., Luo, B., and Zhai, C.: Characteristics and origins of carbonaceous aerosol in the Sichuan Basin, China[J],
425 Atmos. Environ., 94, 215-223, <https://doi.org/10.1016/j.atmosenv.2014.05.037>, 2014.
- 426 Chen, Y., Zhao, C., Zhang, Q., Deng, Z., Huang, M., and Ma, X.: Aircraft study of ~~Mountain-mountain Chimney-chimney~~
427 ~~Effect-effect~~ of Beijing, China[J], J. Geophys. Res., 114, n/a-n/a, <https://doi.org/10.1029/2008JD010610>, 2009.
- 428 Chen, Z. H., Cheng, S. Y., Li, J. B., Guo, X. R., Wang, W. H., and Chen, D. S.: Relationship between atmospheric pollution
429 processes and synoptic pressure patterns in northern China[J], Atmos. Environ., 42, 6078-6087,

430 <https://doi.org/10.1016/j.atmosenv.2008.03.043>, 2008.

431 Chow, J. C., Watson, J. G., Mauderly, J. L., Costa, D. L., Wyzga, R. E., Vedal, S., Hidy, G. M., Altshuler, S. L., Marrack, D.,
432 Heuss, J. M., Wolff, G. T., Arden Pope III, C., and Dockery, D. W.: Health ~~Effects-effects~~ of ~~Fine-fine~~ Particulate
433 particulate Air-air Pollution: Lines that ~~Connectconnect~~[J], J. Air Waste Manage. Assoc., 56, 1368-1380,
434 <https://doi.org/10.1080/10473289.2006.10464545>, 2006.

435 Deng, T., Wu, D., Deng, X., Tan, H., Li, F., and Liao, B.: A vertical sounding of severe haze process in Guangzhou area[J],
436 Sci. China Earth Sci., 57, 2650-2656, [10.1007/s11430-014-4928-y](https://doi.org/10.1007/s11430-014-4928-y), 2014.

437 Feng, X., Liu, C., Fan, G., Liu, X., and Feng, C.: Climatology and ~~Structures-structures~~ of ~~Southwest-southwest~~ Vortices
438 vortices in the NCEP Climate Forecast System Reanalysis[J], J. Climate., 29, 7675-7701,
439 <https://doi.org/10.1175/jcli-d-15-0813.1>, 2016.

440 Fu, S., Sun, J., Zhao, S., and Li, W.: The energy budget of a southwest vortex with heavy rainfall over south China[J], Adv.
441 Atmos. Sci., 28, 709-724, <https://doi.org/10.1007/s00376-010-0026-z>, 2011.

442 Gao, Y., Liu, X., Zhao, C., and Zhang, M.: Emission controls versus meteorological conditions in determining aerosol
443 concentrations in Beijing during the 2008 Olympic Games[J], Atmos. Chem. Phys., 11, 12437-12451,
444 <https://doi.org/10.5194/acp-11-12437-2011>, 2011.

445 Gu, Y., and Yim, S. H. L.: The air quality and health impacts of domestic trans-boundary pollution in various regions of
446 China[J], Environ. Int., 97, 117-124, <https://doi.org/10.1016/j.envint.2016.08.004>, 2016.

447 Guo, J., Deng, M., Lee, S. S., Wang, F., Li, Z., Zhai, P., Liu, H., Lv, W., Yao, W., and Li, X.: Delaying precipitation and
448 lightning by air pollution over the Pearl River Delta. Part I: Observational analyses[J], J. Geophys. Res.-Atmos., 121,
449 6472-6488, <https://doi.org/10.1002/2015JD023257>, 2016a.

450 Guo, J., Miao, Y., Zhang, Y., Liu, H., Li, Z., Zhang, W., He, J., Lou, M., Yan, Y., Bian, L., and Zhai, P.: The climatology of
451 planetary boundary layer height in China derived from radiosonde and reanalysis data[J], Atmos. Chem. Phys., 16,
452 13309-13319, <https://doi.org/10.5194/acp-16-13309-2016>, 2016b.

453 Guo, Y., Zeng, H., Zheng, R., Li, S., Barnett, A. G., Zhang, S., Zou, X., Huxley, R., Chen, W., and Williams, G.: The
454 association between lung cancer incidence and ambient air pollution in China: A spatiotemporal analysis[J], Environ.
455 Res., 144, 60-65, <https://doi.org/10.1016/j.envres.2015.11.004>, 2016c.

456 He, H., Tie, X., Zhang, Q., Liu, X., Gao, Q., Li, X., and Gao, Y.: Analysis of the causes of heavy aerosol pollution in Beijing,
457 China: A case study with the WRF-Chem model[J], Particuology, 20, 32-40,
458 <https://doi.org/10.1016/j.partic.2014.06.004>, 2015.

459 He, J., Gong, S., Yu, Y., Yu, L., Wu, L., Mao, H., Song, C., Zhao, S., Liu, H., Li, X., and Li, R.: Air pollution characteristics
460 and their relation to meteorological conditions during 2014–2015 in major Chinese cities[J], Environ. Pollut., 223,
461 484-496, <https://doi.org/10.1016/j.envpol.2017.01.050>, 2017.

462 Hu, X.-M., Ma, Z., Lin, W., Zhang, H., Hu, J., Wang, Y., Xu, X., Fuentes, J. D., and Xue, M.: Impact of the Loess Plateau on
463 the atmospheric boundary layer structure and air quality in the North China Plain: A case study[J], Sci. Total Environ.,
464 499, 228-237, <https://doi.org/10.1016/j.scitotenv.2014.08.053>, 2014.

465 Huang, K., Zhuang, G., Lin, Y., Wang, Q., Fu, J. S., Zhang, R., Li, J., Deng, C., and Fu, Q.: Impact of anthropogenic
466 emission on air quality over a megacity – revealed from an intensive atmospheric campaign during the Chinese Spring
467 Festival[J], *Atmos. Chem. Phys.*, 12, 11631-11645, <https://doi.org/10.5194/acp-12-11631-2012>, 2012.

468 Huang, Q., Cai, X., Song, Y., and Zhu, T.: Air stagnation in China (1985–2014): climatological mean features and trends[J],
469 *Atmos. Chem. Phys.*, 17, 7793-7805, <https://doi.org/10.5194/acp-17-7793-2017>, 2017.

470 Ji, D., Li, L., Wang, Y., Zhang, J., Cheng, M., Sun, Y., Liu, Z., Wang, L., Tang, G., Hu, B., Chao, N., Wen, T., and Miao, H.:
471 The heaviest particulate air-pollution episodes occurred in northern China in January, 2013: Insights gained from
472 observation[J], *Atmos. Environ.*, 92, 546-556, <https://doi.org/10.1016/j.atmosenv.2014.04.048>, 2014.

473 Ji, D., Wang, Y., Wang, L., Chen, L., Hu, B., Tang, G., Xin, J., Song, T., Wen, T., Sun, Y., Pan, Y., and Liu, Z.: Analysis of
474 heavy pollution episodes in selected cities of northern China[J], *Atmos. Environ.*, 50, 338-348,
475 <https://doi.org/10.1016/j.atmosenv.2011.11.053>, 2012.

476 Kuo, Y.-H., Cheng, L., and Anthes, R. A.: Mesoscale ~~Analyses-analyses~~ of the Sichuan ~~Flood-flood Catastrophecatastrophe~~,
477 11–15 July 1981[J], *Mon. Wea. Rev.*, 114, 1984-2003,
478 [https://doi.org/10.1175/1520-0493\(1986\)114<1984:maotsf>2.0.co;2](https://doi.org/10.1175/1520-0493(1986)114<1984:maotsf>2.0.co;2), 1986.

479 Kuo, Y.-H., Cheng, L., and Bao, J.-W.: Numerical ~~Simulation-simulation~~ of the 1981 Sichuan ~~Floodflood~~. Part I: Evolution
480 of a ~~Mesoscale—mesoscale Southwest—southwest Vortexvortex~~[J], *Mon. Wea. Rev.*, 116, 2481-2504,
481 [https://doi.org/10.1175/1520-0493\(1988\)116<2481:nsotsf>2.0.co;2](https://doi.org/10.1175/1520-0493(1988)116<2481:nsotsf>2.0.co;2), 1988.

482 Langrish, J. P., Li, X., Wang, S., Lee, M. M. Y., Barnes, G. D., Miller, M. R., Cassee, F. R., Boon, N. A., Donaldson, K., Li, J.,
483 Li, L., Mills, N. L., Newby, D. E., and Jiang, L.: Reducing ~~Personal—personal Exposure—exposure~~ to ~~Particulate~~
484 ~~particulate Air—air Pollution—pollution Improves—improves Cardiovascular—cardiovascular Health—health~~ in ~~Patients~~
485 ~~patients~~ with ~~Coronary—coronary Heart—heart Disease~~~~disease~~[J], *Environ Health Perspect.*, 120, 367-372,
486 <https://doi.org/10.1289/ehp.1103898>, 2012.

487 Leng, C., Duan, J., Xu, C., Zhang, H., Wang, Y., Wang, Y., Li, X., Kong, L., Tao, J., Zhang, R., Cheng, T., Zha, S., and Yu, X.:
488 Insights into a historic severe haze event in Shanghai: synoptic situation, boundary layer and pollutants[J], *Atmos.*
489 *Chem. Phys.*, 16, 9221-9234, <https://doi.org/10.5194/acp-16-9221-2016>, 2016.

490 Leśniok, M., Małarzewski, Ł., and Niedźwiedz, T.: Classification of circulation types for Southern Poland with an
491 application to air pollution concentration in Upper Silesia[J], *Phys. Chem. Earth Parts A B C.*, 35, 516-522,
492 <https://doi.org/10.1016/j.pce.2009.11.006>, 2010.

493 Li, L., and Chan, P. W.: LIDAR observation and numerical simulation of vortex/wave shedding at the ~~Eastern—eastern~~
494 ~~Runway—runway Corridor—corridor~~ of the Hong Kong ~~International—international Airportairport~~[J], *Meteorol. Appl.*, 23,
495 379-388, <https://doi.org/10.1002/met.1562>, 2016.

496 Li, L., Li, J., Xin, L., Li, H., and Wei, Q.: Analysis of atmospheric air pollution of Beijing City in Spring Festival period[J],
497 *China Environ. Sci.*, 26, 537-541 (in Chinese), http://manu36.magtech.com.cn/Jweb_zghjkx/CN/2006.

498 Li, Y., Chen, Q., Zhao, H., Wang, L., and Tao, R.: Variations in PM₁₀, PM_{2.5} and PM_{1.0} in an ~~Urban—urban Area—area~~ of the
499 Sichuan Basin and ~~Their—their Relation—relation~~ to ~~Meteorological—meteorological Factors~~~~factors~~[J], *Atmosphere.*, 6, 150,

2015.

- Li, Y., Yan, J., and Sui, X.: Tropospheric temperature inversion over central China[J], *Atmos. Res.*, 116, 105-115, <https://doi.org/10.1016/j.atmosres.2012.03.009>, 2012.
- Liao, T., Wang, S., Ai, J., Gui, K., Duan, B., Zhao, Q., Zhang, X., Jiang, W., and Sun, Y.: Heavy pollution episodes, transport pathways and potential sources of PM_{2.5} during the winter of 2013 in Chengdu (China)[J], *Sci. Total Environ.*, 584-585, 1056-1065, <https://doi.org/10.1016/j.scitotenv.2017.01.160>, 2017.
- Lim, S. S., Vos, T., Flaxman, A. D., Danaei, G., Shibuya, K., Adair-Rohani, H., AlMazroa, M. A., Amann, M., Anderson, H. R., Andrews, K. G., Aryee, M., Atkinson, C., Bacchus, L. J., Bahalim, A. N., Balakrishnan, K., Balmes, J., Barker-Collo, S., Baxter, A., Bell, M. L., Blore, J. D., Blyth, F., Bonner, C., Borges, G., Bourne, R., Boussinesq, M., Brauer, M., Brooks, P., Bruce, N. G., Brunekreef, B., Bryan-Hancock, C., Bucello, C., Buchbinder, R., Bull, F., Burnett, R. T., Byers, T. E., Calabria, B., Carapetis, J., Carnahan, E., Chafe, Z., Charlson, F., Chen, H., Chen, J. S., Cheng, A. T.-A., Child, J. C., Cohen, A., Colson, K. E., Cowie, B. C., Darby, S., Darling, S., Davis, A., Degenhardt, L., Dentener, F., Des Jarlais, D. C., Devries, K., Dherani, M., Ding, E. L., Dorsey, E. R., Driscoll, T., Edmond, K., Ali, S. E., Engell, R. E., Erwin, P. J., Fahimi, S., Falder, G., Farzadfar, F., Ferrari, A., Finucane, M. M., Flaxman, S., Fowkes, F. G. R., Freedman, G., Freeman, M. K., Gakidou, E., Ghosh, S., Giovannucci, E., Gmel, G., Graham, K., Grainger, R., Grant, B., Gunnell, D., Gutierrez, H. R., Hall, W., Hoek, H. W., Hogan, A., Hosgood, H. D., Hoy, D., Hu, H., Hubbell, B. J., Hutchings, S. J., Ibeanusi, S. E., Jacklyn, G. L., Jasrasaria, R., Jonas, J. B., Kan, H., Kanis, J. A., Kassebaum, N., Kawakami, N., Khang, Y.-H., Khatibzadeh, S., Khoo, J.-P., Kok, C., Laden, F., Lalloo, R., Lan, Q., Lathlean, T., Leasher, J. L., Leigh, J., Li, Y., Lin, J. K., Lipshultz, S. E., London, S., Lozano, R., Lu, Y., Mak, J., Malekzadeh, R., Mallinger, L., Marcenes, W., March, L., Marks, R., Martin, R., McGale, P., McGrath, J., Mehta, S., Memish, Z. A., Mensah, G. A., Merriman, T. R., Micha, R., Michaud, C., Mishra, V., Hanafiah, K. M., Mokdad, A. A., Morawska, L., Mozaffarian, D., Murphy, T., Naghavi, M., Neal, B., Nelson, P. K., Nolla, J. M., Norman, R., Olives, C., Omer, S. B., Orchard, J., Osborne, R., Ostro, B., Page, A., Pandey, K. D., Parry, C. D. H., Passmore, E., Patra, J., Pearce, N., Pelizzari, P. M., Petzold, M., Phillips, M. R., Pope, D., Pope, C. A., Powles, J., Rao, M., Razavi, H., Rehfuess, E. A., Rehm, J. T., Ritz, B., Rivara, F. P., Roberts, T., Robinson, C., Rodriguez-Portales, J. A., Romieu, I., Room, R., Rosenfeld, L. C., Roy, A., Rushton, L., Salomon, J. A., Sampson, U., Sanchez-Riera, L., Sanman, E., Sapkota, A., Seedat, S., Shi, P., Shield, K., Shivakoti, R., Singh, G. M., Sleet, D. A., Smith, E., Smith, K. R., Stapelberg, N. J. C., Steenland, K., Stöckl, H., Stovner, L. J., Straif, K., Straney, L., Thurston, G. D., Tran, J. H., Van Dingenen, R., van Donkelaar, A., Veerman, J. L., Vijayakumar, L., Weintraub, R., Weissman, M. M., White, R. A., Whiteford, H., Wiersma, S. T., Wilkinson, J. D., Williams, H. C., Williams, W., Wilson, N., Woolf, A. D., Yip, P., Zielinski, J. M., Lopez, A. D., Murray, C. J. L., and Ezzati, M.: A comparative risk assessment of burden of disease and injury attributable to 67 risk factors and risk factor clusters in 21 regions, 1990–2010: a systematic analysis for the Global Burden of Disease Study 2010[J], *Lancet.*, 380, 2224-2260, [https://doi.org/10.1016/S0140-6736\(12\)61766-8](https://doi.org/10.1016/S0140-6736(12)61766-8), 2012.
- Liu, S., Liu, Z., Li, J., Wang, Y., Ma, Y., Sheng, L., Liu, H., Liang, F., Xin, G., and Wang, J.: Numerical simulation for the coupling effect of local atmospheric circulations over the area of Beijing, Tianjin and Hebei Province[J], *Sci. China Ser.*

535 D Earth Sci., 52, 382-392, <https://doi.org/10.1007/s11430-009-0030-2>, 2009.

536 Lu, C., Deng, Q.-h., Liu, W.-w., Huang, B.-l., and Shi, L.-z.: Characteristics of ventilation coefficient and its impact on urban
537 air pollution[J], J. Cent. South Univ., 19, 615-622, [10.1007/s11771-012-1047-9](https://doi.org/10.1007/s11771-012-1047-9), 2012.

538 Luo, M., Hou, X., Gu, Y., Lau, N.-C., and Yim, S. H.-L.: Trans-boundary air pollution in a city under various atmospheric
539 conditions[J], Sci. Total Environ., 618, 132-141, <https://doi.org/10.1016/j.scitotenv.2017.11.001>, 2018.

540 Luo, Y., Lu, D., Zhou, X., Li, W., and He, Q.: Characteristics of the spatial distribution and yearly variation of aerosol optical
541 depth over China in last 30 years[J], J. Geophys. Res., 106, 14501-14513, <https://doi.org/10.1029/2001JD900030>, 2001.

542 MEP: China National Ambient Air Quality Standards, MEP, Beijing, China, 2012.

543 Miao, Y., Liu, S., Zheng, Y., Wang, S., Chen, B., Zheng, H., and Zhao, J.: Numerical study of the effects of local atmospheric
544 circulations on a pollution event over Beijing–Tianjin–Hebei, China[J], J. Environ. Sci., 30, 9-20,
545 <https://doi.org/10.1016/j.jes.2014.08.025>, 2015.

546 Ni, C., Li, G., and Xiong, X.: Analysis of a vortex precipitation event over Southwest China using AIRS and in situ
547 measurements[J], Adv. Atmos. Sci., 34, 559-570, <https://doi.org/10.1007/s00376-016-5262-4>, 2017.

548 Ning, G., Wang, S., Ma, M., Ni, C., Shang, Z., Wang, J., and Li, J.: Characteristics of air pollution in different zones of
549 Sichuan Basin, China[J], Sci. Total Environ., 612, 975-984, <https://doi.org/10.1016/j.scitotenv.2017.08.205>, 2018.

550 Peng, X., and Cheng, L.: A case numerical study on the evolution of the plateau-east-side low vortex and shear line. Part
551 I: Analysis and diagnosis[J], J. Lanzhou Univ. Nat. Sci., 28, 163-168,
552 <https://doi.org/10.13885/j.issn.0455-2059.1992.02.029>, 1992.

553 Qu, Y., Han, Y., Wu, Y., Gao, P., and Wang, T.: Study of PBLH and ~~Its~~ its ~~Correlation~~ correlation with ~~Particulate~~ particulate
554 ~~Matter~~ matter from ~~Oneone-Year-year~~ Observation-observation over Nanjing, Southeast China[J], Remote Sens., 9, 668,
555 2017.

556 Quan, J., Gao, Y., Zhang, Q., Tie, X., Cao, J., Han, S., Meng, J., Chen, P., and Zhao, D.: Evolution of planetary boundary
557 layer under different weather conditions, and its impact on aerosol concentrations[J], Particuology., 11, 34-40,
558 <https://doi.org/10.1016/j.partic.2012.04.005>, 2013.

559 Shi, Y., Zhang, N., Gao, J., Li, X., and Cai, Y.: Effect of fireworks display on perchlorate in air aerosols during the Spring
560 Festival[J], Atmos. Environ., 45, 1323-1327, <https://doi.org/10.1016/j.atmosenv.2010.11.056>, 2011.

561 Slingo, J. M.: The ~~Development~~ development and ~~Verification~~ verification of ~~A-a~~ Cloud-cloud ~~Prediction-prediction~~ Scheme
562 ~~scheme~~ For—for the ~~Eemwf—~~ ECWmf Model[J], Q. J. Roy. Meteor. Soc., 113, 899-927,
563 <https://doi.org/10.1002/qj.49711347710>, 1987.

564 Tang, G., Zhu, X., Hu, B., Xin, J., Wang, L., M ünk el, C., Mao, G., and Wang, Y.: Impact of emission controls on air quality in
565 Beijing during APEC 2014: ~~H~~ idar ceilometer observations[J], Atmos. Chem. Phys., 15, 743-750,
566 <https://doi.org/10.5194/acp-15-12667-2015>, 2015.

567 Tao, J., Cheng, T., Zhang, R., Cao, J., Zhu, L., Wang, Q., Luo, L., and Zhang, L.: Chemical composition of PM_{2.5} at an urban
568 site of Chengdu in southwestern China[J], Adv. Atmos. Sci., 30, 1070-1084, <https://doi.org/10.1007/s00376-012-2168-7>,
569 2013a.

570 Tao, J., Zhang, L., Engling, G., Zhang, R., Yang, Y., Cao, J., Zhu, C., Wang, Q., and Luo, L.: Chemical composition of PM_{2.5}
571 in an urban environment in Chengdu, China: Importance of springtime dust storms and biomass burning[J], *Atmos. Res.*,
572 122, 270-283, <https://doi.org/10.1016/j.atmosres.2012.11.004>, 2013b.

573 Tao, M., Chen, L., Su, L., and Tao, J.: Satellite observation of regional haze pollution over the North China Plain[J], *J.*
574 *Geophys. Res.-Atmos.*, 117, n/a-n/a, 10.1029/2012JD017915, 2012.

575 Tao, M., Chen, L., Xiong, X., Zhang, M., Ma, P., Tao, J., and Wang, Z.: Formation process of the widespread extreme haze
576 pollution over northern China in January 2013: Implications for regional air quality and climate[J], *Atmos. Environ.*, 98,
577 417-425, <https://doi.org/10.1016/j.atmosenv.2014.09.026>, 2014.

578 Tian, P., Cao, X., Zhang, L., Sun, N., Sun, L., Logan, T., Shi, J., Wang, Y., Ji, Y., Lin, Y., Huang, Z., Zhou, T., Shi, Y., and
579 Zhang, R.: Aerosol vertical distribution and optical properties over China from long-term satellite and ground-based
580 remote sensing[J], *Atmos. Chem. Phys.*, 17, 2509-2523, <https://doi.org/10.5194/acp-17-2509-2017>, 2017.

581 Wang, Q.-W., and Tan, Z.-M.: Multi-scale topographic control of southwest vortex formation in Tibetan Plateau region in an
582 idealized simulation[J], *J. Geophys. Res.-Atmos.*, 119, 11,543-511,561, <https://doi.org/10.1002/2014JD021898>, 2014.

583 Wang, T., Nie, W., Gao, J., Xue, L. K., Gao, X. M., Wang, X. F., Qiu, J., Poon, C. N., Meinardi, S., Blake, D., Wang, S. L.,
584 Ding, A. J., Chai, F. H., Zhang, Q. Z., and Wang, W. X.: Air quality during the 2008 Beijing Olympics: secondary
585 pollutants and regional impact[J], *Atmos. Chem. Phys.*, 10, 7603-7615, <https://doi.org/10.5194/acp-10-7603-2010>,
586 2010.

587 Wang, X., Dickinson, R. E., Su, L., Zhou, C., and Wang, K.: PM_{2.5} ~~Pollution-pollution~~ in China and ~~How-how It-it Has-has~~
588 ~~Been-been Exacerbated-exacerbated~~ by ~~Terrain-terrain~~ and ~~Meteorological-meteorological~~ ~~Conditionsconditions~~[J], *Bull.*
589 *Am. Meteorol. Soc.*, 99, 105-119, <http://dx.doi.org/10.1175/BAMS-D-16-0301.1>, 2018.

590 Wang, Y., Hao, J., McElroy, M. B., Munger, J. W., Ma, H., Chen, D., and Nielsen, C. P.: Ozone air quality during the 2008
591 Beijing Olympics: ~~effectiveness-Effectiveness~~ of emission restrictions[J], *Atmos. Chem. Phys.*, 9, 5237-5251,
592 <https://doi.org/10.5194/acp-9-5237-2009>, 2009.

593 Wang, Y., Yao, L., Wang, L., Liu, Z., Ji, D., Tang, G., Zhang, J., Sun, Y., Hu, B., and Xin, J.: Mechanism for the formation of
594 the January 2013 heavy haze pollution episode over central and eastern China[J], *Sci. China Earth. Sci.*, 57, 14-25,
595 <https://doi.org/10.1007/s11430-013-4773-4>, 2014.

596 Wang, Y., Zhuang, G., Xu, C., and An, Z.: The air pollution caused by the burning of fireworks during the lantern festival in
597 Beijing[J], *Atmos. Environ.*, 41, 417-431, <https://doi.org/10.1016/j.atmosenv.2006.07.043>, 2007.

598 Wei, P., Cheng, S., Li, J., and Su, F.: Impact of boundary-layer anticyclonic weather system on regional air quality[J], *Atmos.*
599 *Environ.*, 45, 2453-2463, <https://doi.org/10.1016/j.atmosenv.2011.01.045>, 2011.

600 Whiteman, C. D., Hoch, S. W., Horel, J. D., and Charland, A.: Relationship between particulate air pollution and
601 meteorological variables in Utah's Salt Lake Valley[J], *Atmos. Environ.*, 94, 742-753,
602 <https://doi.org/10.1016/j.atmosenv.2014.06.012>, 2014.

603 Wu, P., Ding, Y., and Liu, Y.: Atmospheric circulation and dynamic mechanism for persistent haze events in the
604 Beijing-Tianjin-Hebei region[J], *Adv. Atmos. Sci.*, 34, 429-440, <https://doi.org/10.1007/s00376-016-6158-z>, 2017.

605 Yang, L., Wu, Y., Davis, J. M., and Hao, J.: Estimating the effects of meteorology on PM_{2.5} reduction during the 2008
606 Summer Olympic Games in Beijing, China[J], *Front Environ Sci Eng.*, 5, 331,
607 <https://doi.org/10.1007/s11783-011-0307-5>, 2011.

608 Ye, X., Song, Y., Cai, X., and Zhang, H.: Study on the synoptic flow patterns and boundary layer process of the severe haze
609 events over the North China Plain in January 2013[J], *Atmos. Environ.*, 124, 129-145,
610 <https://doi.org/10.1016/j.atmosenv.2015.06.011>, 2016.

611 Yu, S., Gao, W., Xiao, D., and Peng, J.: Observational facts regarding the joint activities of the southwest vortex and plateau
612 vortex after its departure from the Tibetan Plateau[J], *Adv. Atmos. Sci.*, 33, 34-46,
613 <https://doi.org/10.1007/s00376-015-5039-1>, 2016.

614 Zeng, S., and Zhang, Y.: The ~~Effect-effect~~ of ~~Meteorological-meteorological Elements-elements~~ on ~~Continuing-continuing~~
615 ~~Heavy-heavy Air-air Pollution~~: A ~~Case-case Study-study~~ in the Chengdu ~~Area-area~~ during the 2014 Spring
616 Festival[J], *Atmosphere.*, 8, 71, <https://doi.org/10.3390/atmos8040071>, 2017.

617 Zhang, J., Luo, B., Zhang, J., Ouyang, F., Song, H., Liu, P., Cao, P., Schäfer, K., Wang, S., Huang, X., and Lin, Y.: Analysis
618 of the characteristics of single atmospheric particles in Chengdu using single particle mass spectrometry[J], *Atmos.*
619 *Environ.*, 157, 91-100, <https://doi.org/10.1016/j.atmosenv.2017.03.012>, 2017.

620 Zhang, J. P., Zhu, T., Zhang, Q. H., Li, C. C., Shu, H. L., Ying, Y., Dai, Z. P., Wang, X., Liu, X. Y., Liang, A. M., Shen, H. X.,
621 and Yi, B. Q.: The impact of circulation patterns on regional transport pathways and air quality over Beijing and its
622 surroundings[J], *Atmos. Chem. Phys.*, 12, 5031-5053, <https://doi.org/10.5194/acp-12-5031-2012>, 2012a.

623 Zhang, S.-T., and Niu, S.-j.: ~~Haze-to-fog transformation during a long lasting, low visibility episode in Nanjing~~[J], *J. Trop.*
624 *Meteorol.*, 22, 67-77, <https://doi.org/10.16555/j.1006-8775.2016.S1.007>, 2016.

625 Zhang, X. Y., Wang, Y. Q., Niu, T., Zhang, X. C., Gong, S. L., Zhang, Y. M., and Sun, J. Y.: Atmospheric aerosol
626 compositions in China: ~~spatial~~~~Spatial~~/temporal variability, chemical signature, regional haze distribution and
627 comparisons with global aerosols[J], *Atmos. Chem. Phys.*, 12, 779-799, <https://doi.org/10.5194/acp-12-779-2012>,
628 2012b.

629 Zhang, Z., Zhang, X., Gong, D., Kim, S. J., Mao, R., and Zhao, X.: Possible influence of atmospheric circulations on winter
630 haze pollution in the Beijing–Tianjin–Hebei region, northern China[J], *Atmos. Chem. Phys.*, 16, 561-571,
631 <https://doi.org/10.5194/acp-16-561-2016>, 2016.

632
633

634

Table 1. Overview of the eight heavy air pollution events affected by dry low-pressure systems.

Event	Most polluted city	Heavy air pollution event		Most polluted day			End date of heavy air pollution event			Other cities with heavy air pollution
		Start and end dates of air pollution event	PM ₁₀ concentration range in this period ($\mu\text{g m}^{-3}$)	Date	PM ₁₀ concentration ($\mu\text{g m}^{-3}$)	Visibility (m)	Date	PM ₁₀ concentration ($\mu\text{g m}^{-3}$)	Visibility (m)	
1	Mianyang	13–14 Jan 2006	284–442	13 Jan 2006	442	800	15 Jan 2006	166	12000	Chengdu
2	Chengdu	29 Jan 2006	407	29 Jan 2006	407	<50	30 Jan 2006	190	11000	None
3	Chengdu	19–23 Dec 2006	348–385	23 Dec 2006	385	1500	24 Dec 2006	246	11000	None
4	Chengdu	21–24 Dec 2007	260–529	23 Dec 2007	529	800	25 Dec 2007	174	3000	Mianyang
5	Chengdu	18–20 Jan 2009	264–381	19 Jan 2009	381	<50	21 Jan 2009	220	11000	Mianyang
6	Chengdu	3 Feb 2011	403	3 Feb 2011	403	2000	4 Feb 2011	190	11000	None
7	Chengdu	22–31 Jan 2014	282–562	31 Jan 2014	562	<500	1 Feb 2014	207	2500	Deyang
8	Chengdu	1–6 Jan 2017	294–480	5 Jan 2017	480	100	7 Jan 2017	118	11000	Deyang

635

636

637 **Table 2.** Relative vorticity at 700 hPa during the periods of deteriorating and improving air quality in the eight heavy
638 air pollution events.

639 **Table 2.** Relative vorticity at 700 hPa during the periods of deteriorating and improving air quality in each of the eight
640 heavy air pollution events.

641

Event	Deteriorating air quality		Improving air quality	
	Time (BST)	Relative vorticity ($1 \times 10^{-5} \text{ s}^{-1}$)	Time (BST)	Relative vorticity ($1 \times 10^{-5} \text{ s}^{-1}$)
1	02:00 on 13 Jan 2006	2.58	20:00 on 13 Jan 2006	-0.94
2	02:00 on 29 Jan 2006	4.15	08:00 on 30 Jan 2006	-3.36
3	20:00 on 22 Dec 2006	4.64	14:00 on 23 Dec 2006	-1.09
4	14:00 on 22 Dec 2007	0.59	14:00 on 23 Dec 2007	-0.82
5	02:00 on 19 Jan 2009	1.75	08:00 on 19 Jan 2009	-2.48
6	02:00 on 3 Feb 2011	2.96	14:00 on 3 Feb 2011	3.16
7	02:00 on 31 Jan 2014	9.12	02:00 on 1 Feb 2014	5.49
8	20:00 on 4 Jan 2017	6.49	08:00 on 5 Jan 2017	-5.74

642

643

644 ~~**Table 3. Height of the atmospheric boundary layer (BLH), lower tropospheric stability (LTS), and mean wind speed**~~
645 ~~**(MWS) in the lower troposphere during periods of deteriorating and improving air quality in the eight heavy air**~~
646 ~~**pollution events.**~~

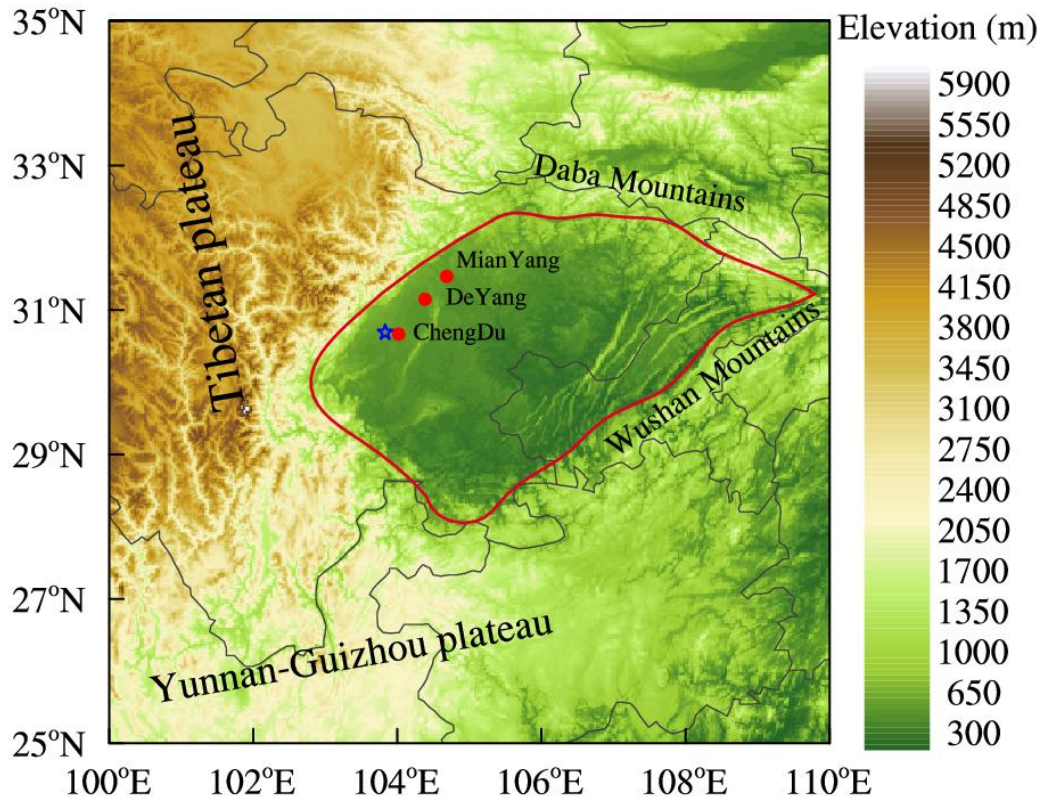
647 **Table 3. Height of the atmospheric boundary layer (BLH), lower tropospheric stability (LTS), and mean wind speed**
648 **(MWS) in the lower troposphere during periods of deteriorating air quality in each of the eight heavy air pollution**
649 **events, and the differences of them between periods of improving and deteriorating air quality in each event.**

650

Event	Deteriorating air quality			Differences between periods of improving and deteriorating air quality		
	BLH (m)	LTS (K)	MWS (m s^{-1})	BLH (m)	LTS (K)	WMS (m s^{-1})
1	278.16	23.13	2.86	144.75	-11.23	0.41
2	375.42	29.45	4.12	139.08	-10.2	1.93
3	279.50	18.54	2.99	-16.45	-5.61	0.34
4	282.61	18.58	1.91	-39.62	-7.23	1.04
5	251.53	19.63	3.11	51.17	-7.88	0.85
6	282.16	25.80	4.22	-16.87	0.55	1.91
7	232.57	25.95	4.21	30.77	-1.97	-1.07
8	266.23	18.88	2.59	107.57	-8.4	0.27

651

652



654

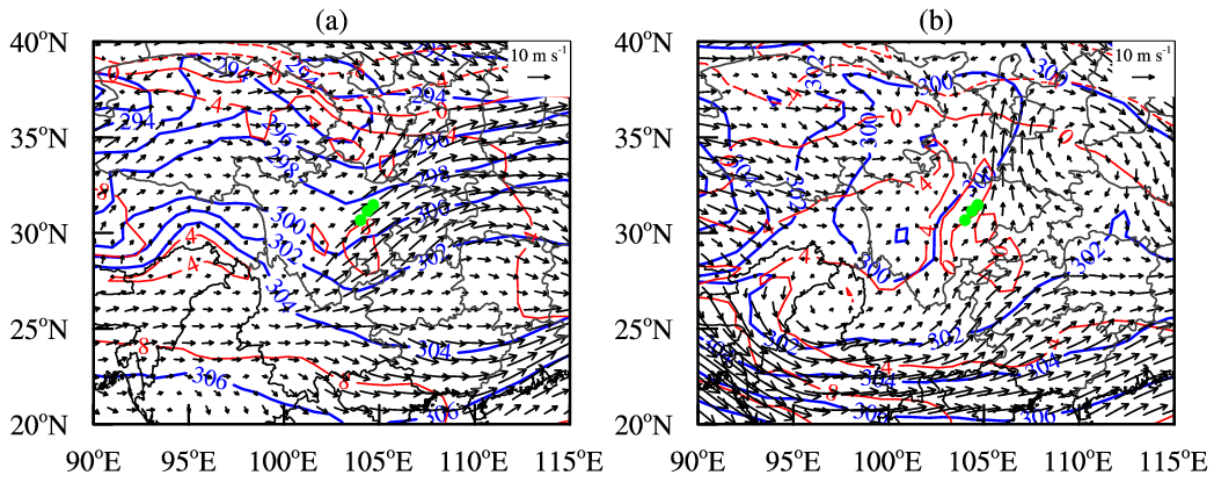
655

656

657

658

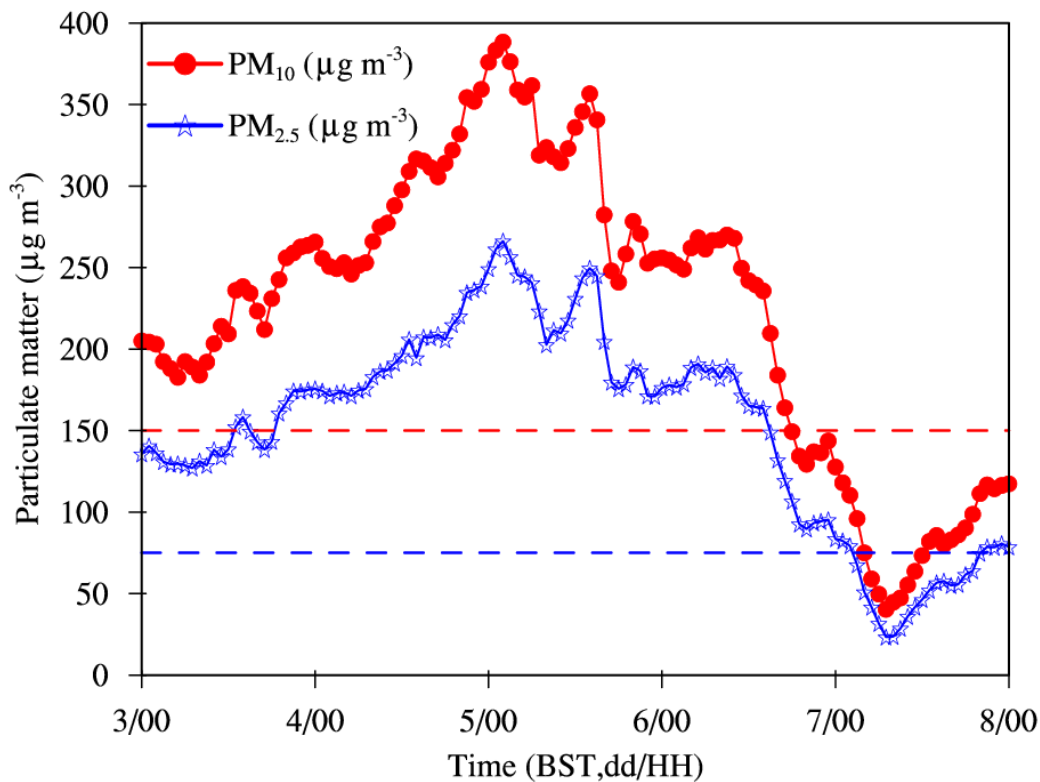
Fig. 1 Topographic map (shading, units: m) of the Sichuan Basin (delineated in red) and surrounding areas showing the location of the cities of Chengdu, Deyang, and Mianyang (red dots). The Wenjiang station is marked with blue five-pointed stars. For interpretation of the colors, see web version of this article.



660

661 **Fig. 2** Weather maps at 700 hPa based on ERA-Interim daily data showing (a) a trough from event 2 at 20:00 BST on
 662 28 January, 2006 and (b) a low vortex from event 4 at 14:00 BST on 22 December, 2007. The blue lines are isopleths
 663 of geopotential height, the red lines are isotherms and the black arrows are wind vectors. The green dots show the
 664 location of the urban agglomeration.

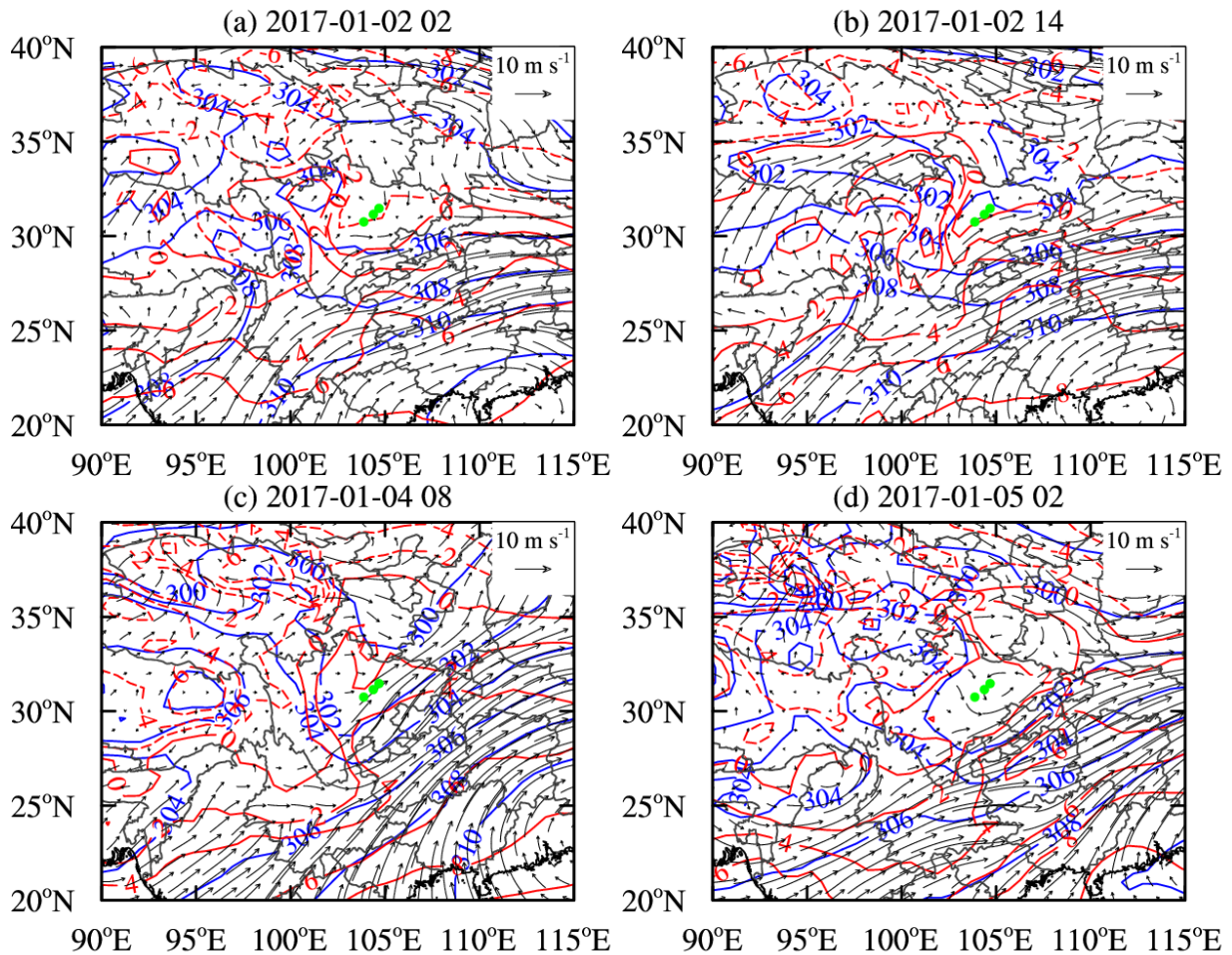
665



667

668 **Fig. 3** Average hourly concentrations of surface PM₁₀ (red solid line) and PM_{2.5} (blue solid line) in the urban
 669 agglomeration from 00:00 BST on 3 January 2017 to 00:00 BST on 8 January 2017 during event 8. The dashed red
 670 line represents Grade II standard of PM₁₀ daily concentration ($150 \mu\text{g m}^{-3}$), the dashed blue line represents Grade II
 671 standard of PM_{2.5} daily concentration ($75 \mu\text{g m}^{-3}$).

672



674

675

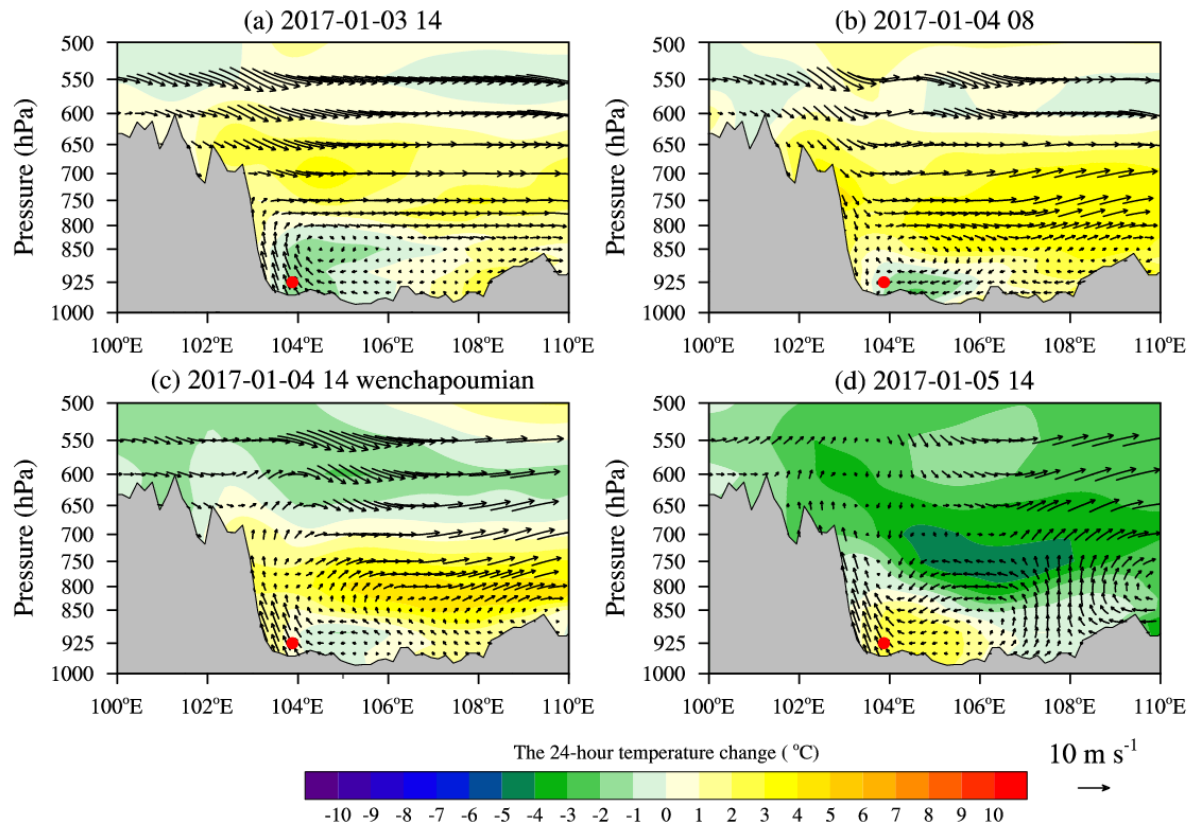
Fig. 4 Weather maps at 700 hPa for event 8 at (a) 02:00 BST on 2 January 2017, (b) 14:00 BST on 2 January 2017, (c) 08:00 BST on 4 January 2017 and (d) 02:00 BST on 5 January 2017. The blue lines are isopleths of geopotential height, the red lines are isotherms and the black arrows are wind vectors. The green dots show the location of the urban agglomeration.

676

677

678

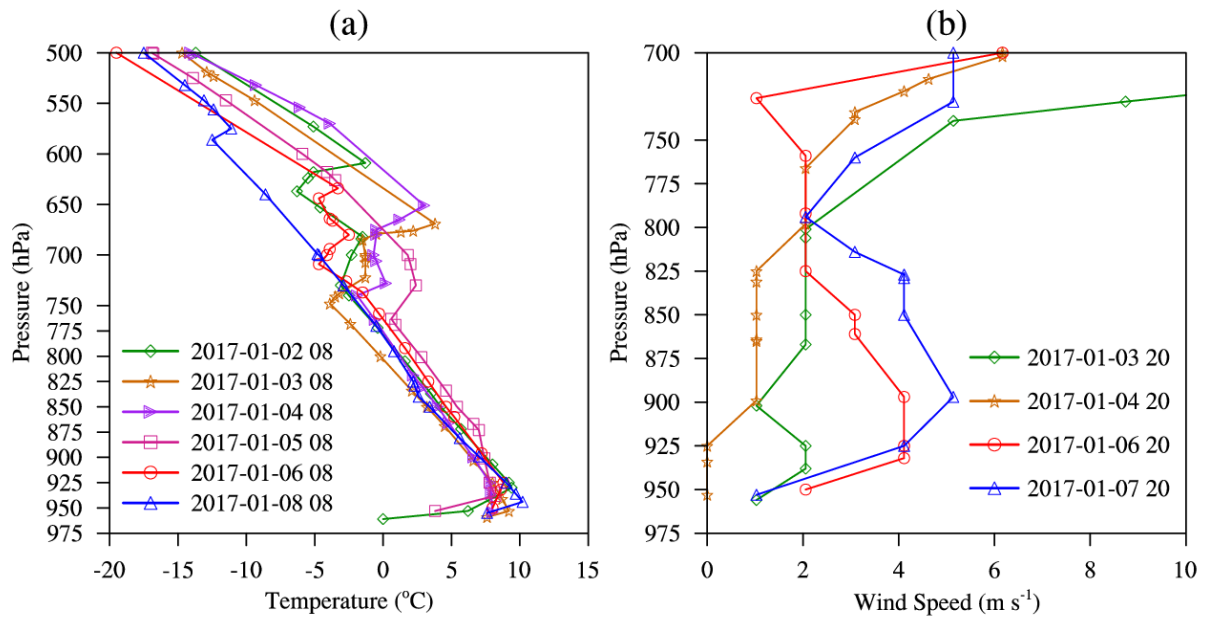
679



681

682 **Fig. 5** West-to-east vertical cross-sections of 24-hour temperature change (shading, units: °C) and wind vectors
 683 (synthesized by u and w) through the most polluted area (30.75 °N) during event 8 at (a) 14:00 BST on 3 January 2017,
 684 (b) 08:00 BST on 4 January 2017, (c) 14:00 BST on 4 January 2017 and (d) 14:00 BST on 5 January 2017 during
 685 event 8. Note that the vertical velocity is multiplied by 100 when plotting the wind vectors. The most polluted area is
 686 marked by red solid dots. The gray shading represents the terrain.

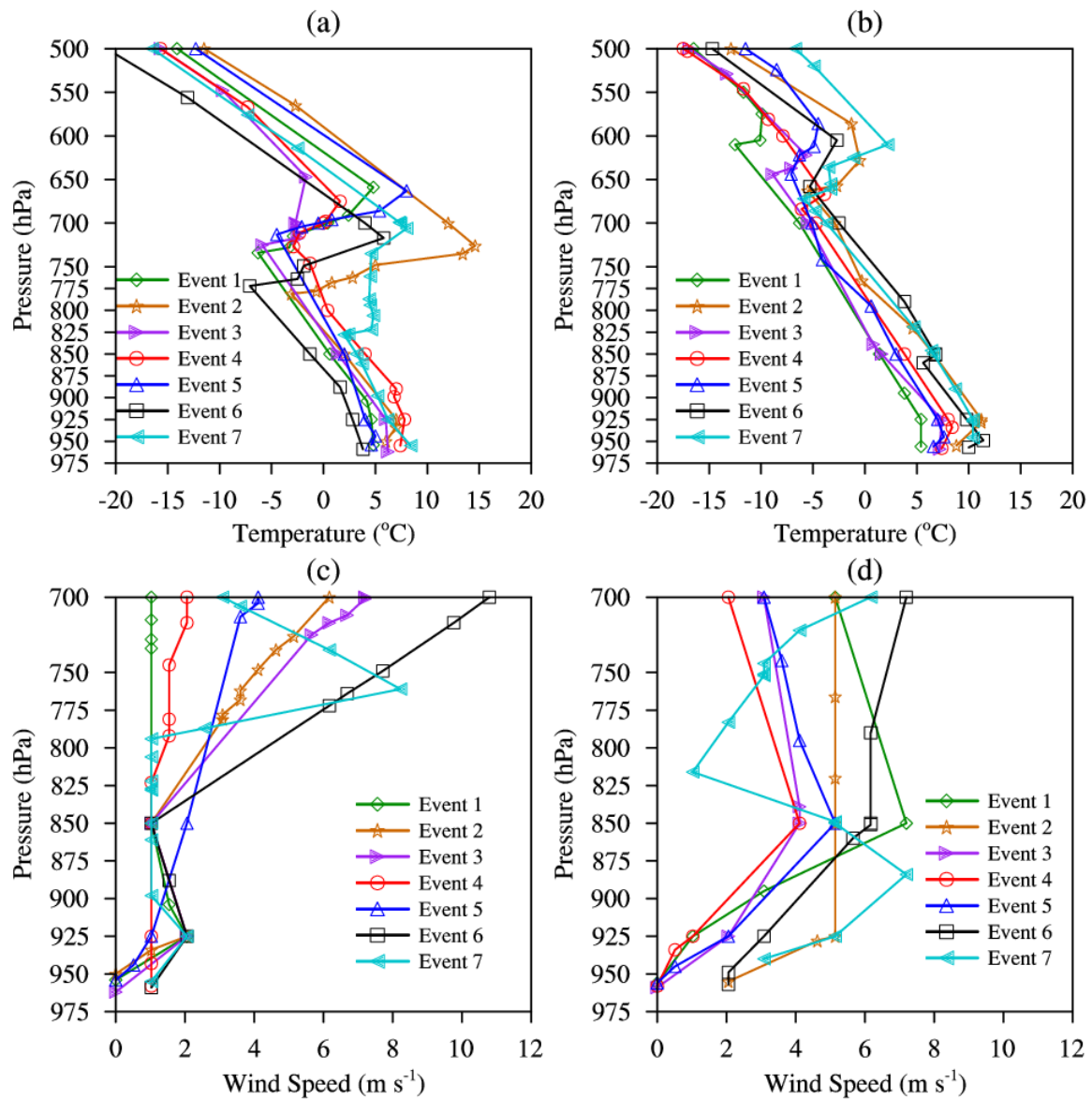
687



689

690 **Fig. 6** Vertical profiles of (a) temperature and (b) horizontal wind speed at Wenjiang station (30.75 °N, 103.875 °E,
 691 see **Fig. 1**) measured by radiosonde during event 8.

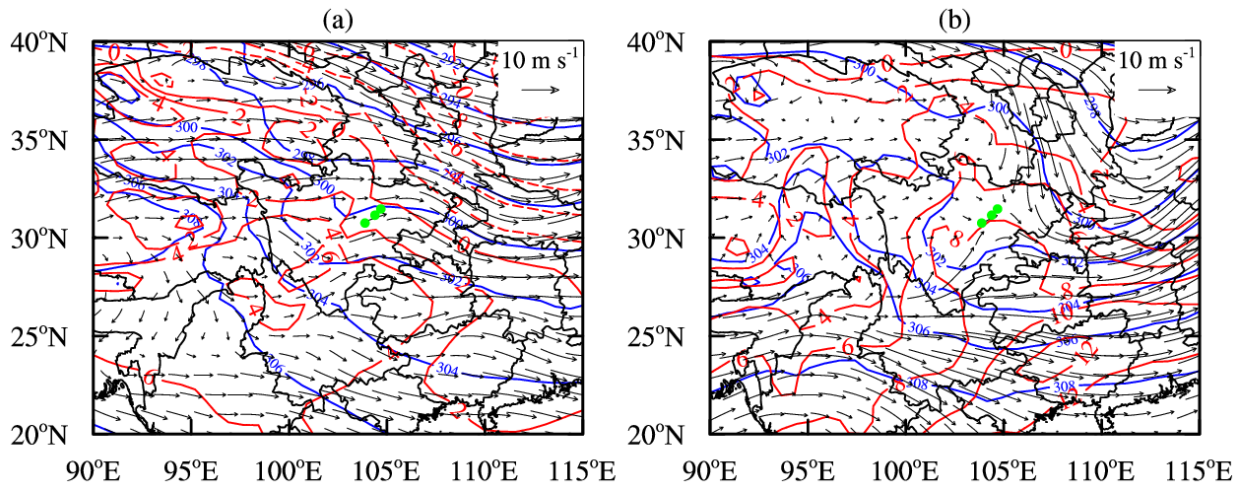
692



694

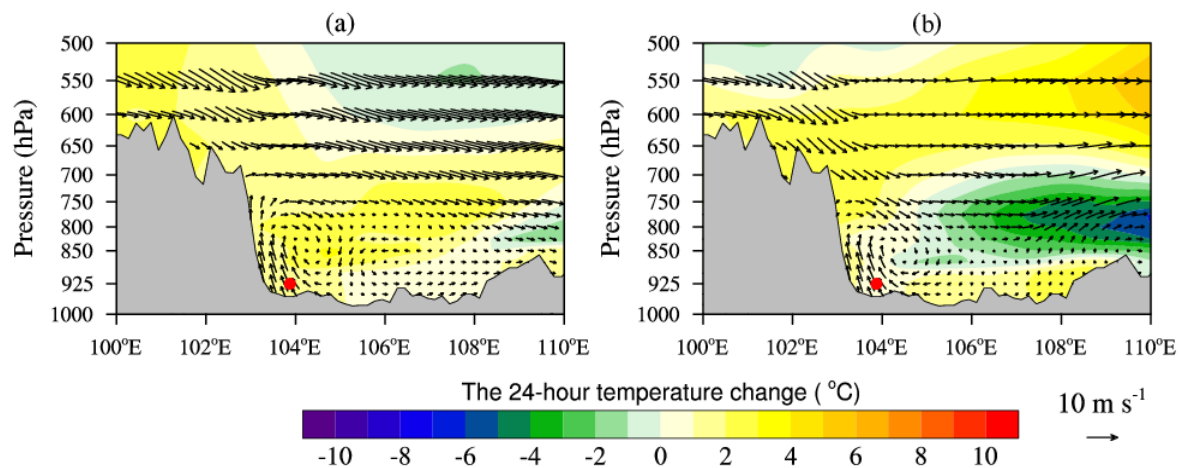
695 **Fig. 7** Vertical profiles of (a) temperature and (c) horizontal wind speed in the urban agglomeration during periods
 696 controlled by the low-pressure system. Vertical profiles of (b) temperature and (d) horizontal wind speed after the
 697 low-pressure system had transited across the urban agglomeration for seven heavy air pollution events (events 1–7).

698



699
700
701
702

Fig. 8 Weather maps at 700 hPa during periods of improving air quality (a) for event 6 and (b) for event 7. The blue lines are isopleths of geopotential height, the red lines are isotherms and the black arrows are wind vectors. The green dots show the location of the urban agglomeration.

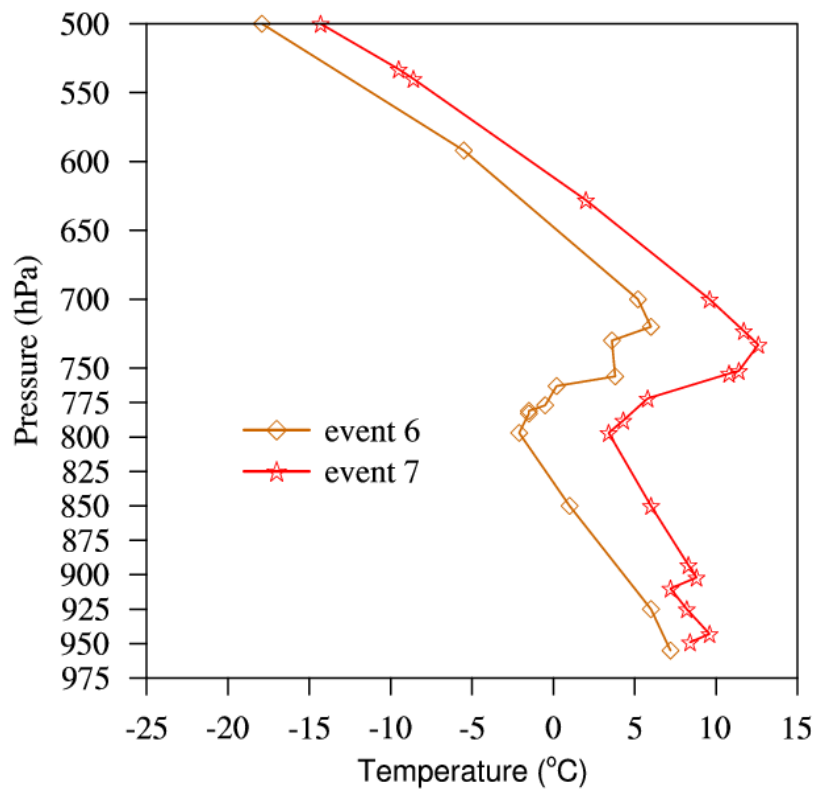


704

705 **Fig. 9** West-to-east vertical cross-sections of 24-hour temperature change (shading, units: °C) and wind vectors
 706 (synthesized by u and w) through the most polluted area (30.75°N) during the periods of improving air quality (a) for
 707 event 6 and (b) for event 7. Note that the vertical velocity is multiplied by 100 when plotting the wind vectors. The
 708 most polluted area is marked by red solid dots. The gray shading represents the terrain.

709

710

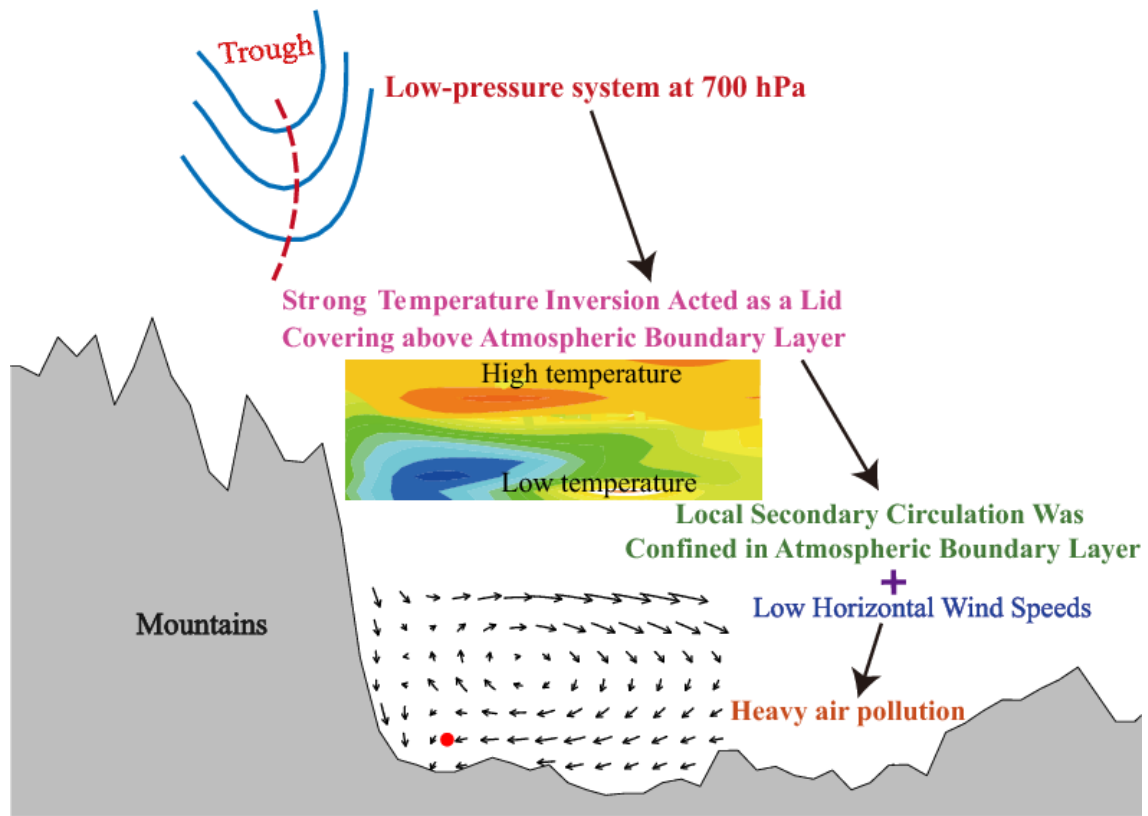


711

712 **Fig. 10** Vertical profiles of temperature at Wenjiang station (30.75 °N, 103.875 °E) measured by radiosonde during
713 periods of improving air quality for event 6 and 7.

714

715



717

718 **Fig. 11** Schematic diagram of the mechanism of influence of a dry low-pressure system on winter heavy air pollution
 719 events in the urban agglomeration.

720

721